Aalto University
School of Engineering

Modeling of dust emission in dimension stone quarry

Suzanne Oudwater
European Mining Course, EMC

Master's Thesis
Espoo 30.09.2017
Supervisor: Prof. Mikael Rinne
Advisor: MSc Marjo Sairanen

Author Suzanne Antonia Oudwater

Title of thesis Modeling of dust emission in dimension stone quarry

Degree programme European Mining, Minerals and Environmental Programme

Major/minor European Mining Course **Code** R3008

Thesis supervisor Prof. Mikael Rinne

Thesis advisor MSc Marjo Sairanen

Date 30/09/2017 **Number of pages** 77 + 11 **Language** English

Abstract

Dust dispersion is a subject that has a large amount of research activity. Most of these researches are focusing on the regions outside the mine or quarry. The dust dispersion model in this research is constructed for industrial purposes, specific for the dust drilling source with closely located receptor points in the quarry. The report has a focus on mining operations in a dimension stone quarry.

This research consists of a literature study about dust behavior, an introduction to the dust dispersion models, regulations and air quality. The research goes more detailed into the mathematical concept of the Gaussian model for the dispersion modeling. Which is widely applied in dust dispersion models, for example AERMOD Breeze and ADMS.

The research about the modeling the dust concentrations in a certain quarry. The quarry Taivassalo is located in the South-West of Finland. The main dust source is from a drilling machine. The observed data from the receptor points are used to compare the modelled results with the measured concentrations and to evaluate the performance of the chosen modeling program. The receptor points were located in the quarry with a distance of 5 m to 60 m from the main dust source.

The research is to indicate the hourly average concentration of PM_{10} (particulate matter with aerodynamic diameter less than 10 microns). The different case studies are chosen to provide scenarios with site specific emission rates. The impact of the different case studies is calculated at the receptor points in the quarry.

The behavior of the predicted data is analyzed by performance modeling, sensitivity analyses and validation curves. This is done to assess the accuracy of the model with the observed data. The drilling emission factor was considered to investigate the observed and predicted PM_{10} concentration.

The results showed that the case studies overpredicted the PM_{10} concentration for all the receptor points. A lower emission factor of the drilling source in the sensitivity analyses gives a better fit compared to the observed data. The sensitivity analyses and decay curve show a stabilization of dust concentration from receptor point of 20 meter onwards.

Keywords Dust dispersion model, Dimension stone, Drilling source, Particle Matter (PM_{10}), Quarry

Acknowledgement

First of all, I want to thank my supervisor, Professor Mikael Rinne and advisor, MSc Marjo Sairanen to make this thesis subject possible and for all their reviews and helpful comments. Marjo was really valuable for me due to her unlimited enthusiasm for providing the input during my research.

My sincere gratitude to Aalto University for funding my research and purchasing the software I needed. Furthermore, I could not imagine the days at office without my office colleagues and all coffee breaks, but most of all their input. Special thanks to my Mexican friends during my stay in Helsinki.

Many thanks to Professor Olavi Selonen and Marjo Sairanen to give a tour in the Quarry and sharing your knowledge. Furthermore, thanks to the team of Breeze Company for answering my questions.

Thanks to Dr. Mike Buxton from TU Delft, for the motivation words on the research.

Above all, I want to thank my family and friends for their unlimited support from the beginning until the end of my studies.

Many thanks and Glück Auf !

Table of Contents

List of Figures

List of Tables

Abbreviations

Abbreviation	Full meaning
AAQSs	Ambient Air Quality Standards
AERMOD	American Meteorological Society/ Environmental Protection Agency Regulatory Model
BSI	British Standard Institute
DW	Down wind
FAC2	Fraction of predictions
FB	Fractional Bias
FDM	Fugitive Dust Model
GM	Geometric Mean Bias
ISO	International Standardization Organization
NA	Not applicable
NAAQS	National Ambient Air Quality Standards
NMSE	Normalized Mean Square Error
OELs	Occupational exposure limits
Particles as PM_{10}	Means particulate matter with an equivalent aerodynamic diameter of 10 micrometers or less
PM	Particulate matter
PM_{10}	Particulate matter with aerodynamic diameter less than 10 microns
SPSs	Source Performance Standards
SW	Side wind
TSP	Total Suspended Particulates

List of Symbols

Symbol	Meaning
%	Percentage
^oC	Celsius
µg	Micrograms
$\mu g/m^3$	Microgram per cubic meters
g/cm^3	Gram per cubic centimeter
g/m^3	Gram per cubic meters
g/s	Grams per second
hr	Hours
kg/m^3	Kilogram per cubic meters
km	Kilometer
km^2	Square kilometer
km^3	Cubic kilometer
m	Meters
m/s	Meters per second
min	Minutes
MPa	Mega Pascal
sec	Seconds
wt%	Percentage by weight

Part I: Introduction

1.1 Background

Quarries and open pits are activities and processes that cause pollution of dust. The sources of dust (particle matter) are generated by the different operations in the mine. The source that generates the dust have a lack of accurate information. There is much unknown information on the specific location of mining operations and equipment (Tartakovsky, et al., 2016). The mining operations generates substantial quantities of airborne respirable dust or inhalable dust. (Lownes, 2008) Heavy machinery is used in the mines to reach the production levels. These production levels have turned into higher results of generating additional dust. (Reed, 2005) Several techniques have been developed to minimalize the dust during the mining activities. The determination of emission rates of various mining activities and prediction of pollutants concentration is necessary to assess the impacts of mining on air quality (Chakraborty, et al., 2002).

The concern exists about the deterioration in environmental quality, especially in the concentration increase of dust dispersion around the mining site. Opencast extraction activities like drilling, blasting, material handling and transport are a potential source of air pollution. (Silvester, et al., 2009) Furthermore, material transfer wind erosion of loose soil, overburden dump and tailings contribute to the air pollution.

To assess the environmental impacts around the mining sites, a detailed model is required for the dust emission. (Vora, 2010) A mathematical dispersion model simulation is an important tool to obtain a better understanding of dust emission and to predict future conditions under various inputs and management decisions. (Chaulya, et al., 2002) Atmospheric dispersion modeling is one of the tools to investigate the dust emission. Parameters of the predicted data such as weather parameters, effective mitigation, and the topography can be used to calculate the dust emission for the area. Atmospheric dispersion modeling is the simulation of the dispersion of the pollutant primary within the boundary layer in the atmosphere. (Cimorelli, et al., 2004)

The study of the transport and dispersion of dust in the atmosphere is crucial for managing and improving the knowledge of the dispersion. It also determines the occurrence and frequencies of the different scenarios of weather and in the end, it enables people to identify the potential hazard areas with these conditions. (Cooper & Alley, 2010)

Open dust sources are sources that generate emissions of solid particles by the forces of wind or machinery acting on the exposed material. Open dust sources include industrial sources of particulate emissions associated with the activities in the open pit. These activities can be open transport, storage, waste aggregate materials, nonindustrial sources such as unpaved roads and parking lots, paved streets and highways, heavy construction activities, and agricultural tilling. (Countess Environmental, 2006)

In the mining field it would be interesting for the operators to have an accurate model to estimate dust emission in various steps of the project. It is essential that the models used to predict the air quality in the nearby environment perform well, because potential over prediction of emission may lead to a denied permit for further mine planning. Therefore, an accurate method of dust emission estimation is needed in the mining industry, aggregate producers, construction sites, civil constructions etc.

In this study, an atmospheric dispersion model, AERMOD is used to predict the dispersion of the ground concentration of PM_{10} (particulate matter with aerodynamic diameter less than 10 microns) at the opencast mine, with specific reference of the mine Taivassalo, Finland. AERMOD is a well validated dispersion simulation software and used worldwide for mining areas.

1.2 Objectives

The goal of this thesis is to provide a modeling practice for the dust dispersion from a drilling source in the dimension stone quarry. The reasons for the research is that there are no prediction models to generate the emission at the rock drilling operation in dimension stone quarries. The model will give more understanding with Gaussian plume dimensions (horizontal, lateral and vertical directions) how the dust will be spreading. Modeling software's are available nowadays and can be used in the mining field. Information about the site, such as topography, is needed to harness the penetration of natural wind systems. The topography gives information about the air change rates within the quarry.

Modeling is to gain knowledge for the industry during the mining operations. It will give more insight into different circumstances. The determination of the emission during the mining activities of the dust concentration is necessary to predict the impacts. The present study aims to reduce the uncertainties on the use of a near-field dispersion at a natural stone quarry in Finland. In this way, a better understanding of dust mass behavior can be achieved. The provided case study is to serve as validation study of the assessment in the article of Sairanen and Selonen (2017).

The implementation of the data in the model ensures that the model will become a tool for understanding the distribution of the dust emission. Eventually the model will be used to analyze the future land use in the surrounding of the mine. In addition, the variation of the model will be investigated with different impacts of the case studies. These case studies will investigate the effects of the dust dispersion of the emission source.

The research question is can we determine if the model predicts the dust dispersion in the quarry?

The three stages are formulated to answer the research question.

1. Evaluation of the PM_{10} concentration at the receptor points in the Taivassalo quarry
2. Investigate with different emission factors for the drilling source
3. Evaluate the model with performance assessment, sensitivity analyses and validation curve the impacts in the design of the dust model emission

With Breeze software is an AERMOD model constructed. The meteorological, topography and dust source parameters are used as input values to present the real situation. Constructing the computer model is an inexpensive method to analyze the dust problems and enables it to compare different case studies with the real life situation. The comparison of the model is to solve the problems related to the physical process. This analysis involves the formulas inserted in the software applied to the model. The output of the dispersion model will be analyzed with the collected data. The model is a tool to determine several input values of independent variables and which will have an impact on the model. A wider use of such advanced sensitivity analysis methods could potentially

be very useful in analyzing and improving the model. Furthermore, the problem areas will be identified with a focus on which physical parameter influences the dust dispersion areas with unavoidable complication.

Changing the physical parameters in the model will be predicting the most and minor influencing factors. The model can give an identification of dust emission in the surrounding of the source in the mining site. Evaluation of dust control techniques by different weather parameters allows to improve the dust control (Vora, 2010). The results from dispersion modeling are used to connect the model with the collected air emission data. The comparison will give an outcome whether the model is suitable to use for the quarry site near-field modelling.

Furthermore, the rock drilling operation is investigated as a source for the dust dispersion in the environment. In the case studies accurate is needed to visualize the impact of the emission in the area. To validate the case studies will be looked into limiting factors of dust emission by Finnish law on the mining site. The generated outcome from the study will be determined with the air quality as used in the literature Holmes and Morawska, (2006).

1.3 Limitations

In the literature, there is much published about atmospheric particle matter implementation of air quality policy (Fuzzi, et al., 2015) The gap in these publications is that the models are mostly gasses and pollution models. The articles do mention some results from the particulate matter (PM), unfortunately, it does not cover the meters close to the breaking source an example is Vora (2010) and Tartakovsky (2016). Therefore, there is not much data from the literature for comparison. However, for dust emissions, any process that can cause the entrainment of dust may be deemed an emission. This may include attrition by the wind of bare ground or stockpiles, site vehicle movements, or mechanical processes. Individual emission sources are therefore rarely measured, and emission factors in the literature often exist as simple estimates based on site size or materials moved. (Bruce, et al., 2016) The second limitation is the physical factors that are inserted in the model. The uncertainties of the input parameters and in which amount they will have an impact on the model. Thirdly, the emission factors of the source will have an impact on the model. These factors also need to be quantified. Furthermore, the error estimation will be taken into account. The major effort in model development, besides extending the range of application, has then tended towards minimizing systematic errors in calculation and in defining the degree of uncertainty associated with model calculations.
This research has emphasized environmental effects caused by dust formed during the quarrying. Health and safety issues of dust concentration are excluded from this research and left out of the scope.

1.4 Outline of the report

The research is divided in four different parts and a short summary of the parts are mentioned.

Part I: Introduction

The research is introduced in this chapter

Part II: Literature study

This chapter focusses on the overview of the literature relating of the subject in the study.

This includes:

- Introduction of the dust dispersion modeling
- Mathematical overview of dust models
- Legislation and quality standards

Part III: Modeling

This part provides an overview of the modeling process and information from the observed data from the Taivassalo quarry. It describes the steps for the different case studies and the details about the implemented topography and meteorology of AERMOD.

Part IV: Results

The results of the modeling are presented in this chapter.

Part V: Discussion

This chapter provides a discussion of the results of the research.

Part VI: Conclusion

A summary of the research findings is presented.

Part VII: Recommendations

This chapter provides future steps and recommendations for this types of studies.

References

A list of references is given in this chapter.

Appendices

Appendix A
Gives an mathematical analyses about the Gaussian dispersion equation

Appendix B
Overview of the meteorological data

Appendix C
Raw data of the receptor points

Appendix D
Parameters for the sensitivity analyses

Appendix E
Figures of the sensitivity analyses

Appendix F
Overview of the validation curves

Appendix G
Analyst Figures of dust dispersion with different emission factors

Part II: Literature study

2.1 Dust behavior

The particle size of dust is very important and many dust properties are depending on atmospheric aerosols. The term aerosols include also the air in which the particles are contained. The determination of the aerosol size distribution is one of the most important aspects involved both in measuring and modeling aerosol dynamics. An overview of the aerosols diameter ranges is given in Figure 1. The figure shows a range from 2 nm up to 100 µm. The aerosols diameter range of 2 nm until 10 µg is a complex mixture of many different chemical species originating from a variety of sources. Particles much greater than 100 µm do not stay airborne long enough to be measured and observed as aerosols. The lower limit is controlled by the gas molecules. This is the smallest entity of the condensed phase that can exist (Lazaridis, 2011). The National Ambient Air Quality Standards (NAAQS) explains that PM stands for particulate matter, also called particle pollution. The particulate matter can be a mixture of solid particles and liquids droplets in the air. This particle pollution includes two regulated particulates, such as PM_{10} and $PM_{2.5}$. PM_{10} are inhalable particles, with diameters that are generally 10 micrometers and smaller. The $PM_{2.5}$ are fine inhalable particles, with diameters that are generally 2.5 micrometers and smaller (The United States Environmental Protection Agency, 2016). The inhalable particles are transported by air movements through the atmosphere. The aerosols arise both from natural sources such as dust from the surface, volcanoes, sea salt and anthropogenic sources such as vehicles emissions, combustion emissions from industry and houses (Lazaridis, 2011). In the literature, the $PM_{2.5}$, $PM_{10,}$ and Total Suspended Particles (TSP) are most commonly used for the particulate matter. According to the International Standardization Organization (ISO) and British Standard Institute (BSI), dust is defined as small solid particles, conventionally below 75 µm in diameter, which settle out under their own weight but which may remain suspended for some time (Petavratzi, et al., 2005). Aerodynamic diameter is defined as the diameter of a hypothetical sphere of density 1 g/cm^3. It has the same terminal velocity in the calm air as the particle of concern, regardless of its geometric size, shape, and density (World Health Organization, 1999).

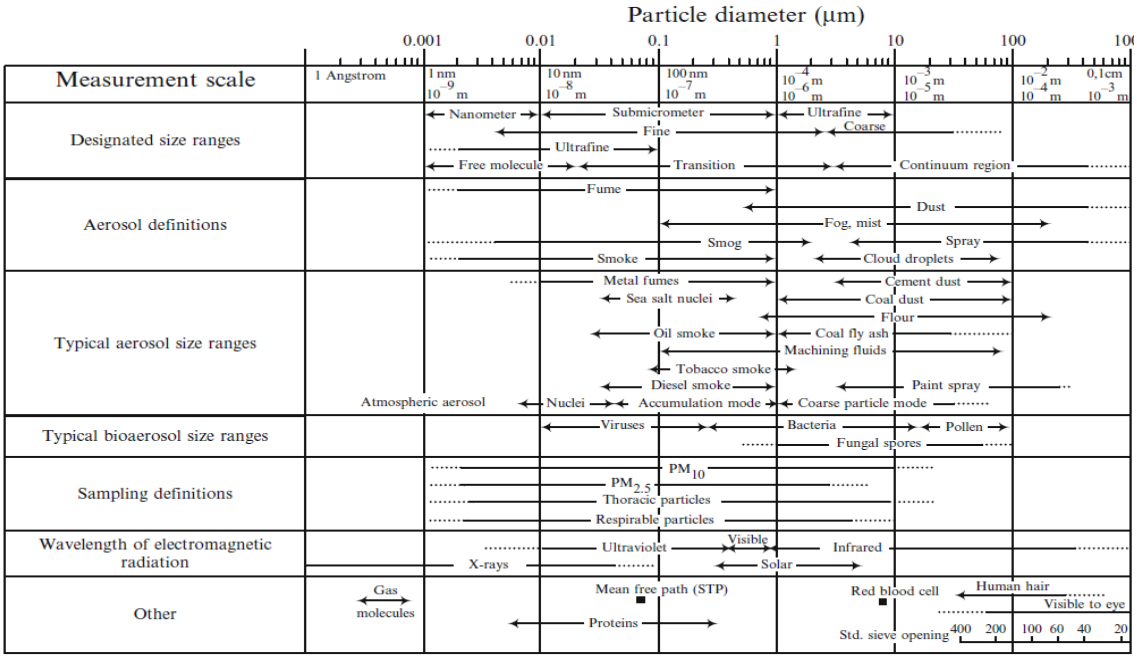

Figure 1: Particle size ranges and definitions for aerosols source: Hinds (1999)

2.2 Introduction to the dispersion modeling

2.2.1 Pollution in the atmosphere

The air pollution models are established with dealing with the elevated background concentrations. The background concentrations are the existing ambient air pollutant concentrations. The existing background concentration can be determined with the containment emission rate, characteristics of the emission source, local topography, meteorology of the area, and operating parameters. (National Institute of Water and Atmospheric Research, 2004) A schematic overview is shown in Figure 2 as the input for the dispersion model. The complexity of the dispersion is considered with the topography and the meteorological data. The meteorological data consist of the wind direction and speed for transport and the turbulence and mixing height in the lower boundary layer. The dispersion modeling uses mathematical equations to influence the pollutant releases and calculate the concentrations. (Holmes & Morawska, 2006)

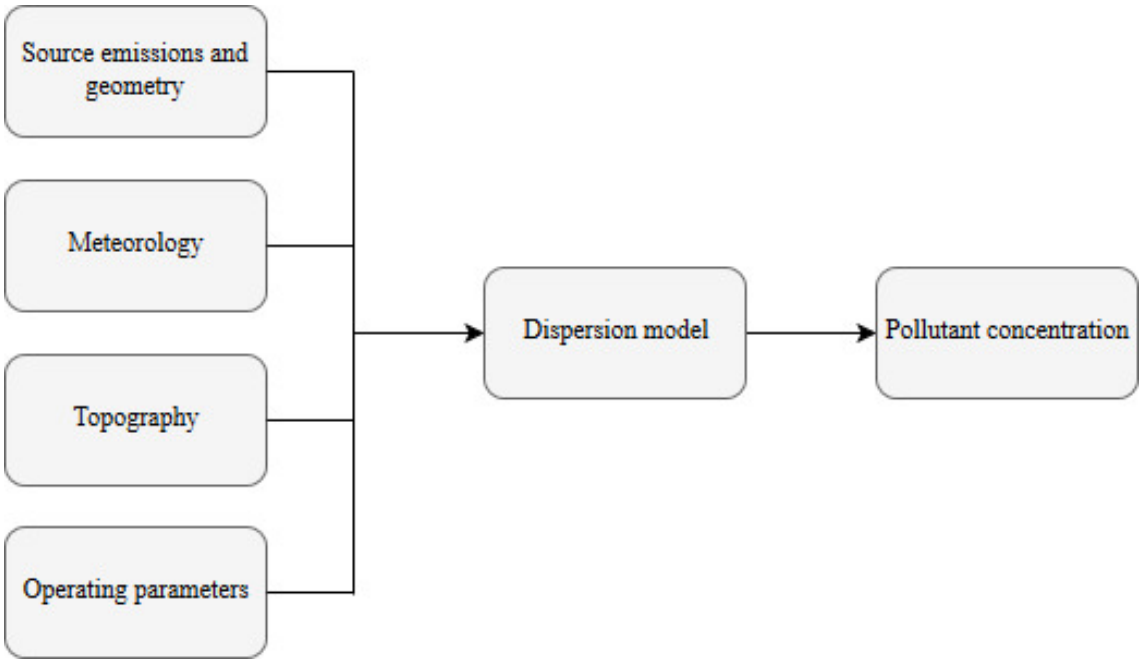

Figure 2: A schematic representation of the input and output of an air dispersion model

2.2.2 Classification by atmospheric stability

Atmospheric stability is a measure propensity for the lateral and vertical motion in the atmosphere. To classify these motions, σ_y (horizontally motion) and σ_z (vertically motion) dispersion information on the weather conditions at the site of the emission is needed. The most commonly used classification of atmospheric stability was developed by Pasquill & Gifford (1961). For both estimations for σ_y and σ_z are shown for the rural situation in Figure 3. The classification has a total of six classes from A through F. With A the most unstable class, D neutral atmosphere, and F the most stable class. These parameters are most usable for releases near the ground. It gives an indication of an unstable atmosphere on sunny days, neutral on overcast days and nights, and stable on clear nights. When the wind increases, the wind speed leads to more neutral conditions. The stability scheme is one of the most accurate formulations of the original Gaussian dispersion model by McElroy & Pooler (1968). In the literature, Pasquill and Gifford used to calculate the plumes such as Tartakovsky et al. (2016) and Lashgari & Kecojevic (2016).

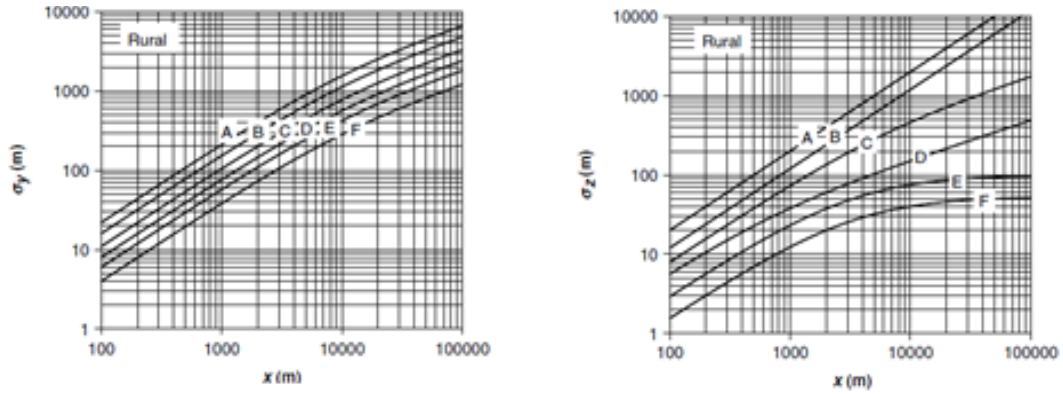

Figure 3: Horizontal (left) and vertical (right) dispersion parameters for a rural terrain. The lines indicate the different classes for the atmosphere, source: Gifford (1976)

2.2.3 Wind roses

Wind roses are graphic tools to show the typical distribution of the wind speed and direction in different situations. Since the wind is circular, it is frequently easier to interpret and visualize the frequency of wind flow subjectively by displaying a wind rose. The wind rose shows the wind frequencies for each direction oriented according to the azimuth for that direction. Figure 4 is a stability wind rose that indicates Pasquill stability class frequencies for each direction. The wind roses in the figure show the various stabilities to be nearly a set proportion of the frequency for that direction. The larger the total frequency for that direction, the greater the frequency for each stability. Since the frequencies of A and B stabilities are quite small. These are 0.72 % and 0.92 % for A and B, respectively. All three unstable classes A, B, and C are added together and indicated by the single line in the figure. (Vallero, 2008)

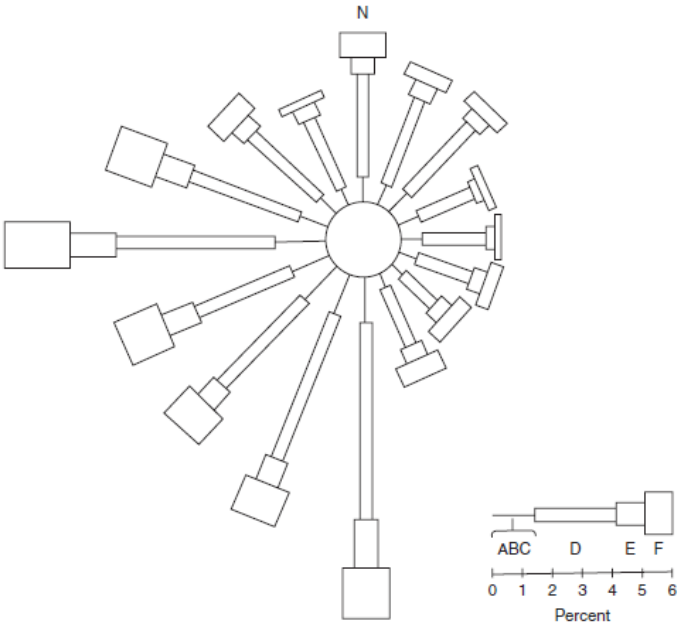

Figure 4: Example of a wind rose with the direction in the Pasquill stability classes source: Vallero (2008)

The wind direction is determined by the initial direction of transport of the dust from the source. The receptor is a location that is receiving the transported dust. It will have a different concentration measurement when the wind direction changes. In Figure 5 shows an one-dimensional grid with an overview of source and receptors. The concentration at the point source is probably more sensitive to wind direction than any other parameter. (Vallero, 2008) Wind speed generally increases with height. One of the effects of wind speed is to dilute continuously released pollutants at the point of emission. (National Institute of Water and Atmospheric Research, 2004)

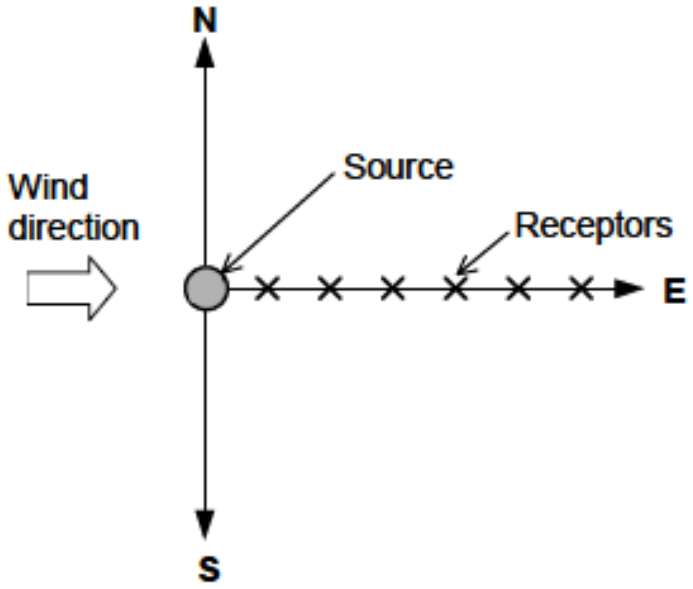

Figure 5: One-dimensional grid to use with a screening meteorological data set, the wind is from one direction only modified from: National Institute of Water and Atmospheric Research (2004)

Whether a source is at the surface or elevated, the dilution takes place in the direction of plume transport. The transportation of the emission is shown in Figure 6 with a dilution by the wind at the emission point. It shows the effect of wind speed for an elevated source with an emission of 6 mass units per second. The figure has two different wind speeds. The wind speed of 6 m/s shows one unit between the vertical parallel planes 1 meter apart. With a slower wind speed of 2 m/s, there are three units between those same vertical parallel planes with 1 meters apart. The wind speeds are being used for the plume dispersion that is estimated as stack top. Wind speed has multiple effects such as the travel time from source to receptor. If the wind speed decreased by two, then the travel time is doubled. For buoyant sources, the plume rise is affected by wind speed. The stronger the wind indicates the conditions for the plume becomes lower. (Vallero, 2008) Specific equations for estimating plume rise are presented in Chapter 2.3.1.

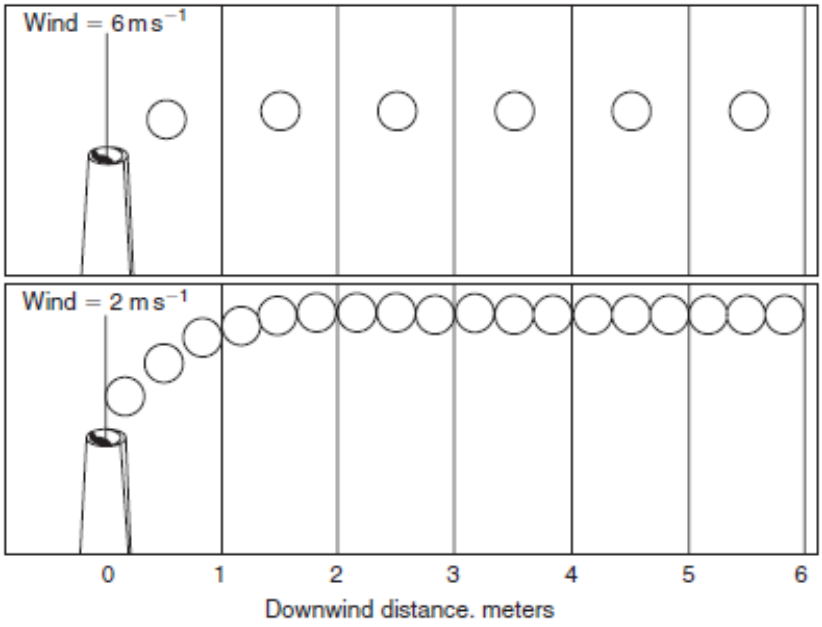

Figure 6: Dilution by wind speed with an emission rate 6 mass units per second source: Vallero (2008)

2.2.4 Previous open pit models

Previous research modeling in mining is done in several fields. In Reed (2005), a research is performed to determine the fugitive dust emission. This fugitive dust can be a result of wind erosion or contaminated soils, equipment or vehicles travel over the roadways. Furthermore, the release from covered landfills, spills, leakage, overburdens and tailings ponds. An overview of these literature categories is given in this subchapter.

Further research is performed in dust dispersion to evaluate a safe distance for equipment in order to avoid overexposure to respirable dust from lead trucks Reed (2005). The dust emission research for digging and loading points in an operating surface coal mine are done by Lashgari & Kecojevic (2016), Chaulya, et al. (2002) and Trivedi et al. (2009). Detailed list of various available engineering controls that may help the mining industry reduce dust exposure is shown in Colinet et al. (2010). An overview of a terrain modeling of fugitive dust emission in quarries is by Chulya et al. (2001), Chakraborty, et al. (2002), Organisack & Reed (2004), Appleton et al. (2006). The particular fugitive emissions due to blasting operations are described in Bhandari (2011) and Jones et al. (2003). On complex terrain and with a variety of wind condition is done by Cui et al. (2011). Studies at dust dispersion at leaching sites, pads of crushed ore is given in Orloff et al. (2006). A detailed research of the mathematical models to simulate the ventilation in open pits is shown in Lownes (2008). The modeling of the overburden and stockpiles in quarry area and the dust emission is done by Appleton et al. (2006) and Chang et al. (2012). Legislation and the equations for an overview of the Gaussian and Lagrangian models are shown in both Reed (2005) and Lownes (2008). Dispersion models have been mostly used for regulatory purposes. These models have adopted a standard modeling procedure in their applications (Behera, et al., 2011). The performance of the model depends on the complexity of the location of the quarry. Additionally, site specific conditions are taken into account to improve the predictions of the AERMOD model. (Tartakovsky, et al., 2016) Studies have shown that the fugitive dust emissions from lower level or in pit sources originates from opencast mining. Other studies showed that the statistical

predictions on these dust emissions where done using other models such as the fugitive dust model (FDM) Chakraborty et al. (2002), Chaulya, et al. (2002) and Prabha & Singh (2006).

2.3 Dust propagation models and mathematical algorithms

2.3.1 Gaussian model algorithm

The Gaussian equations are based on a coordinate scheme with the origin at the ground, *x* downwind from the source, *y* lateral wind, and *z* vertical. The normal vertical distribution near the source is modified at greater downwind distances by eddy reflection at the ground and, when the mixing height is low, by eddy reflection at the mixing height. Eddy reflection refers to the movement away of circular eddies of air from the earth's surface, since it cannot penetrate the surface. (Vallero, 2008) Appendix A is inserted to give in detailed steps the Gaussian equation and more details about the Gaussian plume model.

The air dispersion can be described by equation 1 Reed (2005):

$$x(x,y,z) = \frac{Q}{2\pi u_s \sigma_y \sigma_z}\left(\exp\left\{-0.5\left(\frac{y}{\sigma_y}\right)^2\right\}\right)\exp\left[-0.5\left(\frac{H}{\sigma_z}\right)^2\right] \quad (1)$$

Where x = concentration at downwind distance x ($\mu g/m^3$)

Q = pollutant emission rate (g/sec)

u_s = mean wind speed at release height (m/sec)

σ_y, σ_z = standard deviation of lateral and vertical concentration distribution (m)

y = crosswind distance from the source to the receptor (m)

H = effective height of plume emission (m)

In Figure 7 is the Gaussian atmospheric plume model shown. The sigma σ_y and σ_z are the standard deviations of the horizontal and vertical Gaussian distributions that are used to represent the plume of the pollutant. These coefficients are based upon the atmospheric stability coefficients created by Pasquill and Gifford as described in chapter 2.2.2. In equation 2 of the calculation of pollutant dispersion, assumptions are made for the equation to be valid, such as described in the study of Reed (2005):

1. Emissions must be a constant and uniform
2. Wind direction and speed are constant
3. Downwind diffusion is negligible compared to vertical and crosswind diffusion
4. Terrain is relatively flat
5. There are no crosswind barriers present
6. No deposition or absorption of the pollutant
7. Vertical and crosswind diffusion of the pollutant follow a Gaussian distribution
8. Shape of the plume can be represented by an expanding cone as shown in Figure 7
9. The use of the horizontal and vertical standard deviations, σ_y and σ_z, requires the turbulence of the plume to be homogeneous throughout the entire plume
10. The Gaussian model also has the limitation that it cannot be used for sub-hourly prediction of concentrations as in the study of Collet & Oduyemi (1997)

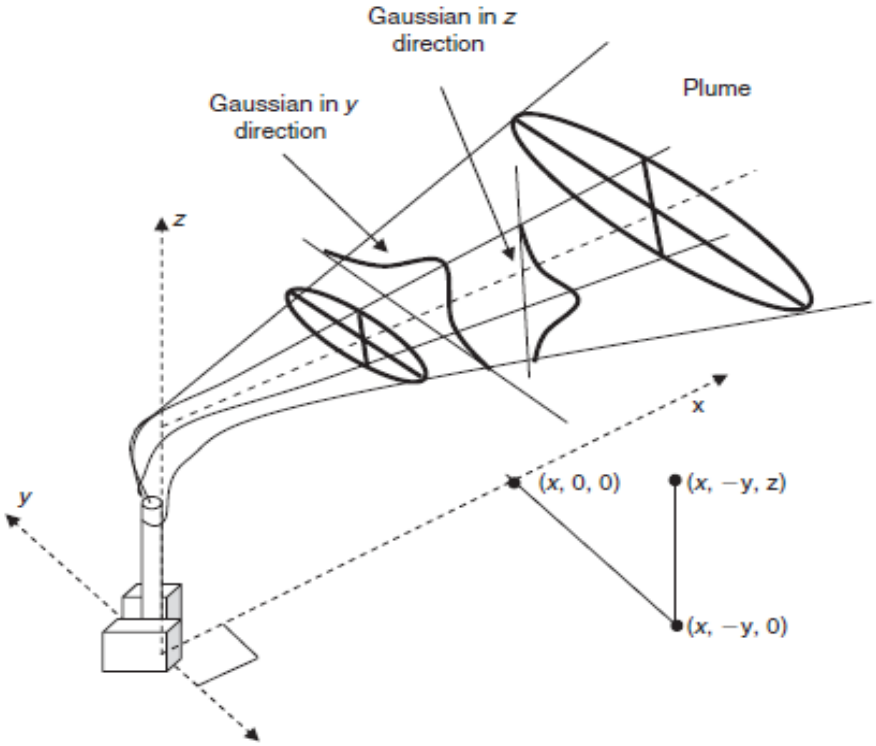

Figure 7: Gaussian atmospheric plume model based on the random distribution in the horizontal and vertical directions. source: Vallero (2008)

2.3.2 Eulerian model algorithm

The Eulerian approach to dispersion modeling solves the conservation of mass equation for a given pollutant species of concentration c. The general form of the equation can be seen in equation 2 of the literature Reed (2005):

$$\frac{\partial\langle c_i\rangle}{\partial t} = -\bar{U}\nabla\langle c_i\rangle - \nabla\langle c_i' U'\rangle + D\nabla^2\langle c_i\rangle + \langle S_i\rangle \qquad (2)$$

Where U = Ū + U’

U = wind field vector U(x,y,z)

Ū = average wind field vector

U’ = fluctuating wind field vector

c = <c> + c’

c = pollutant concentration

< c > = average pollutant concentration; < > denotes average

c’ = fluctuating pollutant concentration

D = molecular diffusivity

S_i = source term

Eulerian models have the disadvantage that their resolution is confined by the spatial and discretization of the mesh on which they are solved. The use of a mesh is computationally expensive and traditionally requires some form of optimization to achieve any degree of efficiency. The approach is information rich, providing a description of the relevant transport dynamics at all defined points throughout the domain (Collett & Oduyemi, 1997).

2.3.3 Model performance assessment

There are several statistical analyses to compare the model performance with the observed data. These statistical indicators are Fractional Bias (FB), Geometric Mean Bias (MG), Normalized Mean Square Error (NMSE), and the fraction of predictions within a factor of two of observations (FAC2). These data plots correlate model predictions with field measurements.

FB is a linear measure and reflects the degree of matching between the predicted and observed mean of the concentration distribution. MG is also linear and reflects the degree of bias of the geometric mean rather than the arithmetic mean. A perfect model would result in MG = 1, whereas with MG<1 is underprediction and MG>1 result is an overprediction (Venkatram, et al., 2013). NMSE measures the relative scatter of the concentration distribution. For the case of the predicted and observed means are equal, an NMSE = 1 indicates that the root mean square error is equal to the mean indicates a factor of 4 and over- or under-prediction of the mean. FAC2 is the most robust measure, as it reflects the percentage of predicted concentrations lying within a factor of two of observations. Time series plots were also used to provide visual insight into models performance in part IV. A good estimation of the predicted and the observed mean is FB in a linear measure. The linearity reflects the degree of matching between the predicted and observed mean of the concentration distribution. It ranges between 2 and -2, with a perfect model resulting in FB = 0. (Ghannam & El-Fadel, 2013)

These data plots correlation model predictions within the field measurement are done by Ghannam & El-Fadel (2013), Demirarslan et al. (2017) and Prabha & Singh (2006). These are shown in equation 3 until 6. Research is done in Curci (2015) for sensitivity analyses on dust at locations all over the world.

$$FB = \frac{(\overline{C_o} - \overline{C_p})}{0.5(\overline{C_o} + \overline{C_p})} \rightarrow \frac{\overline{C_p}}{\overline{C_o}} = \frac{1 - 0.5\,FB}{1 + 0.5FB} \tag{3}$$

$$MG = exp\left(\overline{\ln C_o} - \overline{\ln C_p}\right) \tag{4}$$

$$NMSE = \frac{\overline{(C_o - C_p)^2}}{\overline{C_o}\,\overline{C_p}} \tag{5}$$

FAC2 = Fraction of data satisfying the expression

$$0.5 \leq \frac{C_p}{C_o} \leq 2 \tag{6}$$

Where C_o = observed concentrations

C_p = predicted concentrations

2.4 Federal regulations and quality standards for PM_{10}

2.4.1 Air quality standards for PM_{10}

To ensure the air quality of the European Union the limit values are target on numerous substances, which include particle matter. (Petavratzi, et al., 2005). In Finland, the limit values are determined in the Environmental Action program from the European Union. It is established with the goal: the need to reduce pollution to levels which minimize harmful effects on human health, paying particular attention to sensitive populations, and the environment as a whole, to improve the monitoring and assessment of air quality including the deposition of pollutants and to provide information to the public (European Parliament and the Council, 2008). The Act 2008/50/EC is a directive of the European Parliament that describes the air quality legislation. It includes two limit values for PM_{10} for the protection of the human health, where the PM_{10} is the most upper limit value for the 24 hours mean concentration that cannot cross 50 $\mu g/m^3$. The yearly limit for PM_{10} is set on 40 $\mu g/m^3$. The local, regional and national level have to meet these limits (Directorate General for Environment, 2016).
The approach of the US Congress and the Environmental Protection Agency has the guidelines as the general laws. It allows the agencies to do necessary research and write specific regulations. For the particle matter of 10 micron per cubic meter it has specific standards and the term are those that apply to emissions of pollutants from specific source. They are always written in terms of concentrations ($\mu g/m^3$ or ppm). Note that some states have set their own standards (Cooper & Alley, 2010). A number of countries has stablished their Ambient Air Quality Standards (AAQSs). Also the World Health Organization (WHO) created his guidelines values in the Ambient Air quality Directive. The air quality guidelines of WHO are guidance to policy makers on the reducing effects on the health of air pollution (World Health Organization, 2006). The daily limit of 50 $\mu g/m^3$ cannot be exceed more than 35 days (European Environment Agency, 2016). The limit restrictions of countries and organizations are shown in Table 1.

Table 1: Air quality limit and target values for PM_{10} source: European Union (2008) and WHO (2006)

	Limit concentrations ($\mu g/m^3$)	
Country / Organization	**24-hour mean**	**Annual mean**
Australia	50	-
China	100	150
EU	50[i]	40
Finland	50	40
Scotland	-	18
South Africa	180	60
UK	-	20
NAAQS	150[ii]	-
WHO	50[iii]	20

i. Not to be exceeded more than 35 days per year
ii. Not to be exceeded more than once per year on an average over 3 years
iii. 99th percentile (3 days/year)

Another type of standard is Source Performance Standards (SPSs) which apply to the emissions of pollutants from specific source. It is written in terms of mass emissions per unit of time or unit of production (g/min or kg of pollutant per metric ton of product produced).

Part III: Modeling

3.1 Introduction AERMOD

AERMOD is a steady state Gaussian plume model. Figure 8 shows the flow and processing of information in the AERMOD modeling system. The main program runs on the meteorological preprocessor (AERMET) and a terrain pre-processor (AERMAP). In this study the dust dispersion models AERMOD is used to predict the dispersion of ground concentration of PM_{10} at a quarry for a case study. AERMOD is a well-validated dispersion model and is used worldwide in several studies (EPA, 2016). However, few studies have been conducted in emissions on particles.

The meteorological preprocessor (AERMET) is used to calculate the meteorological parameters for AERMOD in the planetary boundary layer (PBL). The planetary boundary is a layer concept layer into regulatory dispersion model. This ranges from 1 to 2 km during the day. The terrain pre-processor (AERMAP) both characterizes the terrain, and generates receptor grids for the dispersion model (AERMOD) (EPA, 2016).

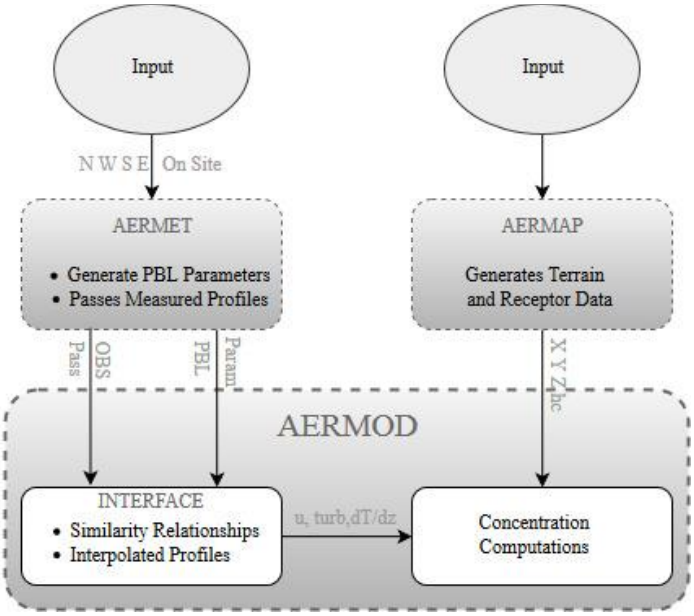

Figure 8: Overview of the data flow in the AERMOD modeling system source: EPA (2016)

AERMET uses meteorological data and surface characteristics to calculate boundary layer parameters needed by AERMOD. The measurement data is used to determine the effects of the atmosphere. This data measured on-site, must be representative of the meteorology in the modeling domain (EPA, 2016). The input for the meteorology are the surface characteristics: albedo, surface roughness and Bowen ratio, plus standard meteorological observations such as wind speed, wind direction, temperature, and cloud cover. AERMET calculates the PBL parameters: friction velocity (u*), Monin-Obukhov length (L), convective velocity scale (w*), temperature scale (θ*), mixing height (z_i), and surface heat flux (H) (Cimorelli, et al., 2004). These parameters are then passed to the AERMOD interface where similarity expressions are used to calculate vertical profiles of wind speed (u), lateral and vertical turbulent fluctuations (σ_v, σ_w), potential temperature

gradient ($d\theta/dz$), and potential temperature (θ). The reference height for wind is at 10 meters and for temperature 2 meters.
The terrain pre-processor AERMAP uses gridded terrain data to calculate a representative terrain-influence height (h_c), also referred to as the terrain height scale. The terrain height scale h_c, which is uniquely defined for each receptor location, is used to calculate the dividing streamline height. It uses gridded terrain data for the modeling area to calculate a representative terrain-influence height associated with each receptor location. The gridded data is supplied to AERMAP in the format of the Digital Elevation Model (DEM) data (USGS, 1994). The terrain preprocessor can also be used to compute elevations for both discrete receptors and receptor grids (EPA, 2016). The base map is created with assigned model objects with their actual elevations. The model objects indicate sources, receptor points and buildings. These two operation types serve different purposes. If the modeling domain is mainly a flat area, model object elevations will not have a big impact on the model results and therefore, running AERMAP is not mandatory. On the other hand, for an area that has complex terrain features, including model object elevations in the model input will improve the accuracy of the modeling results. For each receptor, AERMAP passes the following information to AERMOD: the receptor's location (x_r , y_r), its height above mean sea level (z_r), and the receptor specific terrain height scale (h_c) (EPA, 2016).

The concentrations of PM_{10} from overall emissions as a result of various sources at the pit were simulated for each modeling hour. The input parameters of each source were entered into the model is outlined in Table 2. The following sources were identified and were treated as specified sources as outlined in the case study models in chapter 3.3.

The equations for estimating PM_{10} emitted from different sources used in this study were derived from the literature, USEPA and NPI websites. Since there are no equations specifically developed for the mining in quarries, the equations used were adopted from iron mining due to the availability of this information.

Table 2: Summary of input parameters source: EPA (2004c)

	Input parameters
Point source	Point emission rate in g/s
	Release height above ground in meters
	Exit temperature in degrees K
	Exit velocity in m/s
	Inside diameter
Volume source	Volume emission rate in g/s
	Release height above the ground, in meters
	Initial lateral dimension of the volume in meters
	Initial vertical dimension of the volume in meters
Area source	Area emission rate in $g/(s*m^2)$
	Release height above ground in meters
	Length of X side of the area
	Length of Y side of the area
	Orientation angle for the rectangular area in degrees from north clockwise (optional)

3.2 Observed study

3.2.1 Quarry Taivassalo

The quarry in the area of Taivassalo is located in South West Finland and has a monthly production of 300 m^3. (Sairanen & Selonen, 2017) The quarry is located next to the bay Varkaankarinaukko and it is attached to the Gulf of Bothnia. Measurements of the area of the quarry is 21600 m^2 and roughly -30 meters deep in 2013. The geographical location of the mines is North latitude 60°35'15.72'', East longitude 21°28'25.32'' as shown in Figure 9. The data was processed with surface data of station EFTU in Turku supplemented by cloud cover of the station in Kiikala Airport and upper air data of the station in Jokioinen. The surface station EFTU is located 44 km from the quarry with an elevation of 59 meters. The location of Kiikala airport is 120 km and station Jokioinen is 113 kilometers from the quarry.

Table 3: Coordinates of quarry and weather stations

	X coordinate	Y coordinate
Quarry Taivassalo	525921	6716935
EFTU station	569349	6709322
Kiikala Airport	645772	6704462
Jokioinen station	635956	6745329

Figure 9: Overview of the quarry site and weather stations Jokioinen, EFTU and Kikkala airport modified in Google Earth 2015

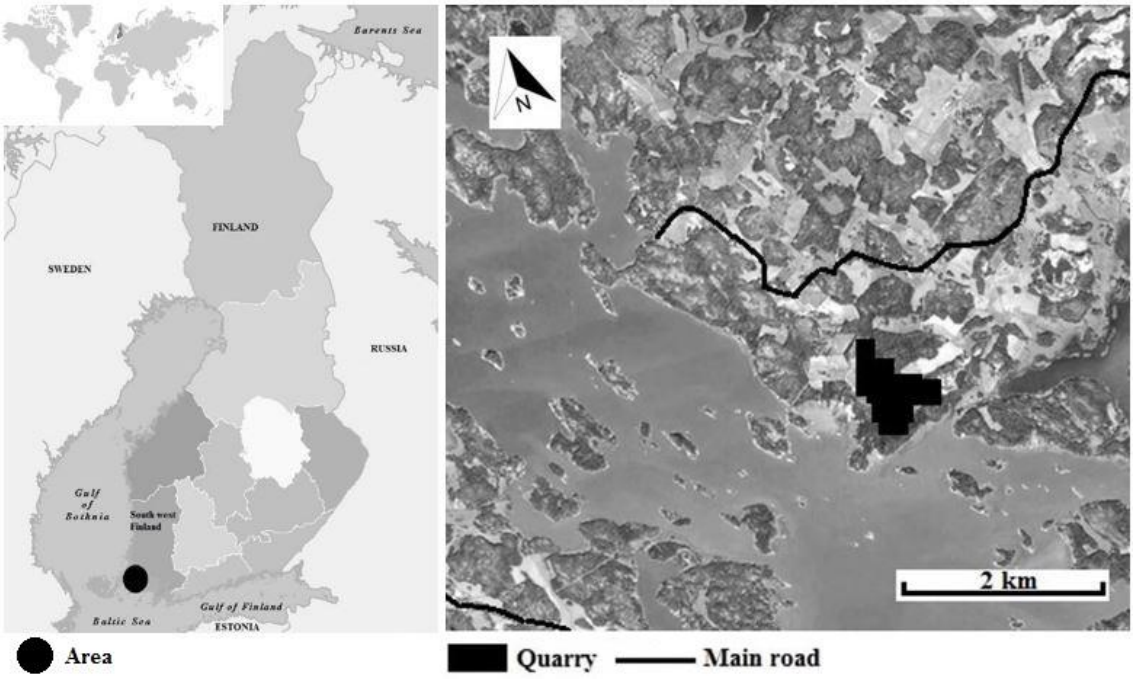

Figure 10: Overview of the quarry site modified from: Google Earth 2015

3.2.2 Production

The mine is producing natural stones with drilling and cutting. The stone blocks are cut or drilled from a solid rock into large solid rectangular blocks with definite dimensions and sizes. Techniques used comprise precision drilling, smooth blasting, wedging, and diamond wire sawing. Figure 11 shows the layout of the quarry showed with two work faces, the haul roads, stockpile, office buildings and waste dump. The two work faces are at two different levels in the quarry and are separated by a wall of 90 degrees. The white lines represent the steep walls of the quarry. The stone block is loaded at the work face and traveled on the haul road to the stockpile. At the stockpiles, the ore blocks are unloaded. Two office buildings are located outside the open pit. The waste dump is located at the east side of the quarry for low-grade material.

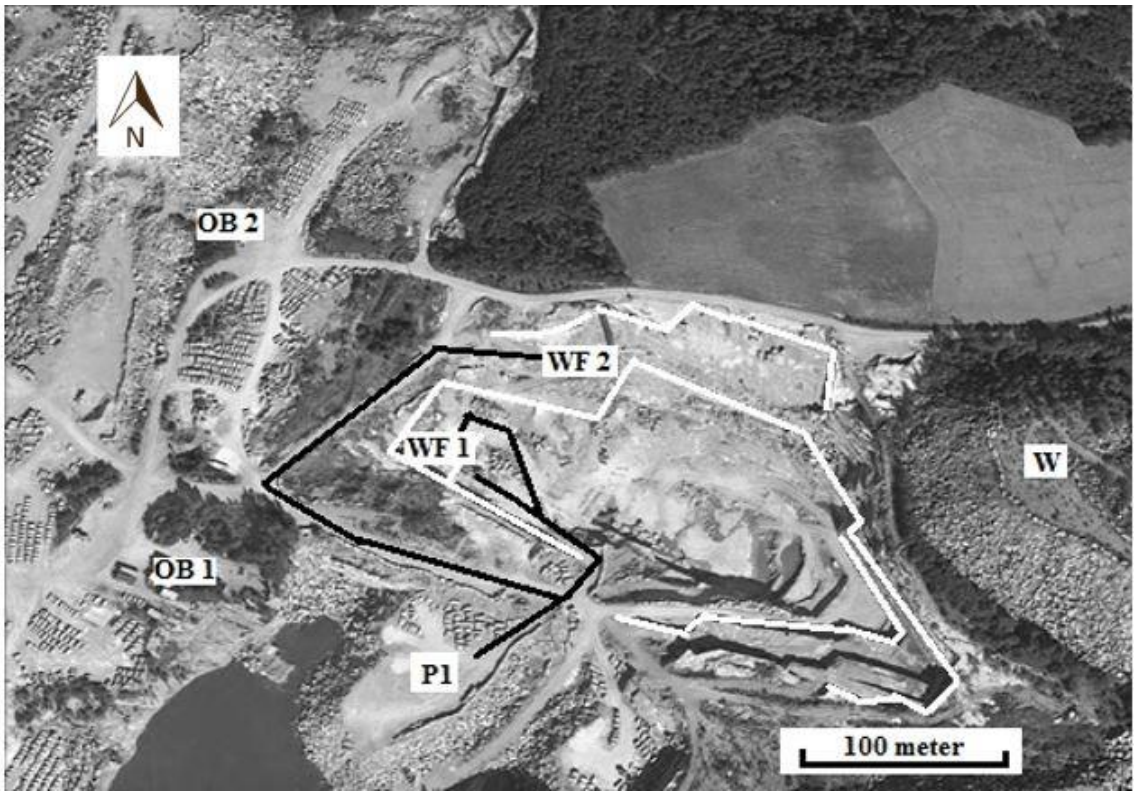

Figure 11: Quarry layout (OB - Office Building; P - Stock Pile; W - Waste dump; WF - Work-Face; black stripe is haul road and white stripe are the 90 degrees walls of the quarry) modified from: Google Earth 2015

The first stage is the detaching of large blocks by drilling. The holes are drilled horizontally, the diameter of 30 mm and 6–8 m long with hydraulic drilling machines as shown in Figure 12. The distances between holes are in average 30 cm. The horizontal holes are charged and blasted with plastic cartridges (K-pipes) with a low average charge density. The extraction comprises of the loosening the primary block of size from 100 to 4000 m^3.The detached primary block is subdivided into smaller blocks, which are further shaped into final sizes and dimensions, mainly by drilling and hydraulic splitting. The final product of the quarry is a stone block with a definite size and shape. After loading the stone block will be taken to the stockpiles. The details about the rock are shown in Table 4. The medium-grained red porphyritic rapakivi granite is mainly composed of potassium feldspar, quartz, plagioclase, and biotite. (Sairanen & Selonen, 2017)

Figure 12: Horizontal drilling with a modified drill from forest machine (D1H) and sampling at downwind (DW) direction at 5 meters distance and side-wind (SW) direction at 10 meter distance source: Sairanen & Selonen (2017)

Table 4: Properties of the rock types source: Sairanen & Selonen, (2017) from Geological Survey of Finland and

Mineral content / technical properties		
Biotite	5.2	wt%
K-Feldspar	39.6	wt%
Muscovite	1.3	wt%
Plagioclase	22.2	wt%
Quartz	30.1	wt%
Accessory minerals	1.8	wt%
Water absorption	0.12	%
Apparent density	2,640	kg/m^3
Flexural strength	13.40	MPa
Frost resistance	-3.7	%
Compressive strength	171	MPa
Abrasion resistance	17	mm

3.2.3 Climate

Climate conditions are important given the importance of mineral dust and climate systems, such as clouds (Bangert, et al., 2012) and weather systems. (Haustein, et al., 2015) To simulate the quarry, the land and meteorlogical properties are needed. The quarry is located in western Finland in an area of forest and agriculture. The rainfall is not consistence during the year and for the months October until April it has snowfall. On average, the mine received 54 mm of rainfall in the year 2013 and 8 cm snow for 5 months. An overview of rainfall and snowfall in Finland is shown in Figure 13 and Figure 14. Figure 13 shows the highest rainfall in mid-autumn (October) and end of the spring (May). The lowest rainfall is recorded at the end of wintertime (February) but it

has the most snowfall days recorded. The peak of the snowfall is recorded in mid-winter (January) with 20 cm.

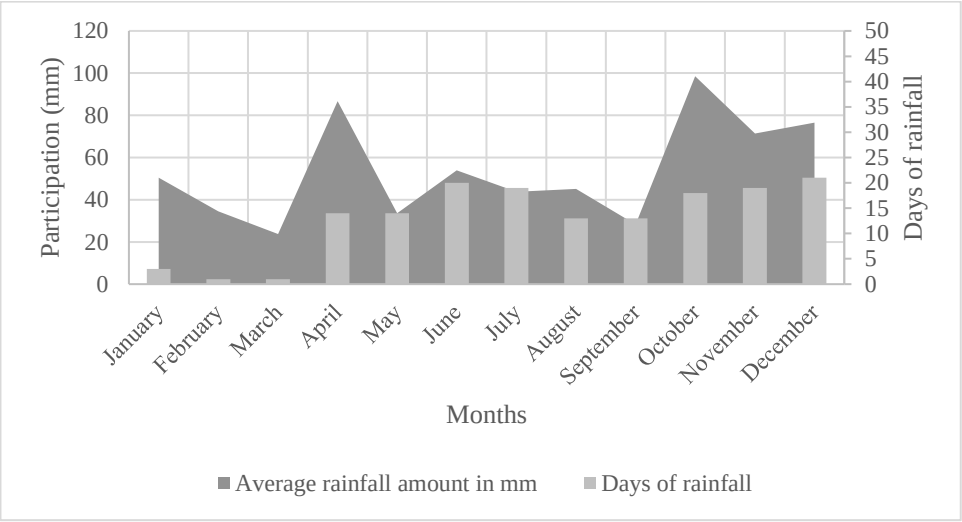

Figure 13: Rainfall overview in 2013 in Finland source: Turku Station (2017)

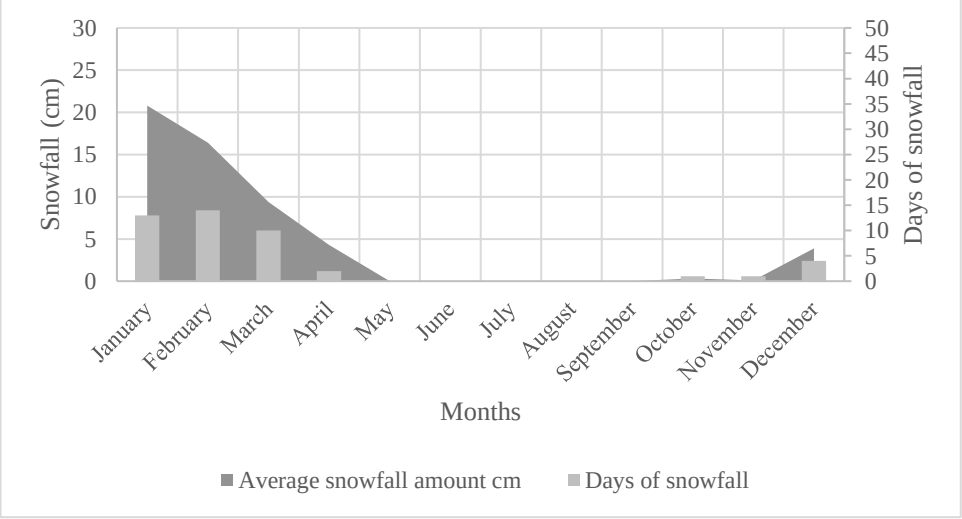

Figure 14: Snowfall overview in 2013 in Finland source: Turku Station (2017)

The wind is predominated in a south-westerly direction. The strongest measurement was made at 16 m/s. The strong north-easterly wind is experienced in quarter 4 of 2013 (October until December). During the study in February and March was a high east wind measured with a wind speed of 11 m/s.
The variation is to be expected at the quarry, but the season's variations are well marked in air temperature. The mean temperature of winter period is - 4 ºC, spring 7 ºC, summer 20 ºC and autumn 7 ºC. During the winter period, the temperature is below zero degrees.

3.2.4 Measurements

The data collection is measured with the nephelometer. The device is shown in Figure 15. The maximum concentration measured for PM_{10} 6,500 µg/m^3 at 5 meters distance from the drilling rig on 01.03.2013. An overview of the minimum and maximum observed data is shown in Table 5 and Table 6.

Table 5: Overview of the minimum and maximum of observed data of PM_{10} (µg/m^3) during 28/02/2013

	Minimum (µg/m^3)	**Maximum (µg/m^3)**
DW 5	4.6	5,456.4
DW 10	2.2	407.7
DW 20	1.9	261.5
DW 30	1.9	117.2
DW 40	1.2	164.3
DW 50	1.8	75.7

Table 6: Overview of the minimum and maximum of observed data of PM_{10} (µg/m^3) during 01/03/2013

	Minimum (µg/m^3)	**Maximum (µg/m^3)**
DW 5	2.6	6,500.0
DW 10	2.3	1,759.7
DW 20	2.8	791.5
DW 30	2.6	134.7
DW 40	2.6	774.0
DW 50	3.7	340.0
DW 60	3.2	514.2

The Turnkey Osiris nephelometer is standardized for a PM_{10} fraction (Turnkey Instruments, 2017) a schematic overview is shown in Figure 16. The measurements were taken during two days during the morning. The time interval is for 5 seconds and is used in order to observe short time variation in dust emissions. The sampling during the drilling was conducted 3 times 5 minutes at each sampling point and 180 measurement results for each size fraction measured, were gained from each sampling point. The sampling duration differed from the planned 15 min in total due to the demands of the drilling procedure was completed. The horizontal drilling is with a speed of 0.14 m/s. (Sairanen & Selonen, 2017)

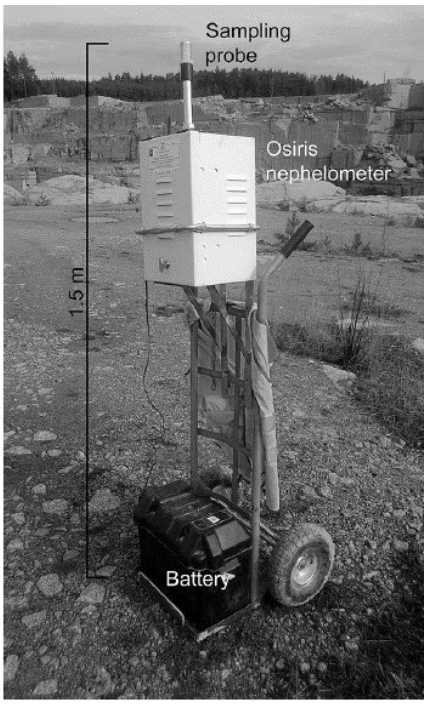

Figure 15: The Osiris nephelometer source: Sairanen & Selonen (2017)

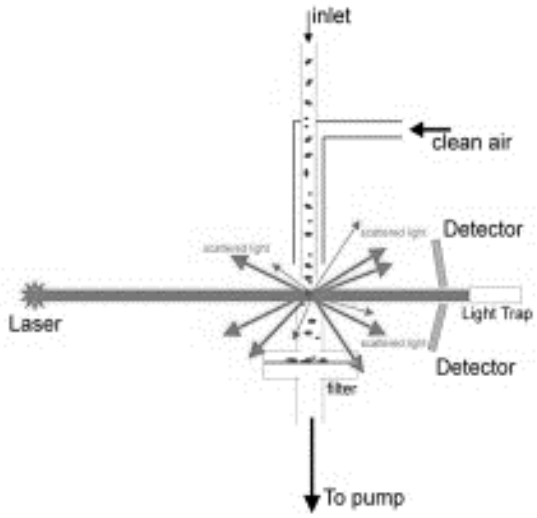

Figure 16: The nephelometer operating principle source: Turnkey Instruments (2017)

3.2.5 Field monitoring

During the mine operation the drilling machine drills with an velocity of 0.14 m/s that generates dust in the quarry. The dust is generated when the blast holes are drilled. The dust mass concentrations were measured near the drill at different distances at downwind (DW) and side-wind (SW) direction, this is shown in Figure 17. The nearest sampling location 5 m at DW direction remained constant during the measurement. The other sampler was relocated to different distances at different wind directions. The sampling height was 1.5 m which represent breathing height as shown in Figure 15. (Sairanen & Selonen, 2017) The overview of the collected data is shown in Figure 18 and Figure 19.

In these figures, the time is on the x as and the concentration measured of the dust in $\mu g/m^3$ on the y-axis. Furthermore, the variation is significant of the short time sampling intervals of 5 seconds.

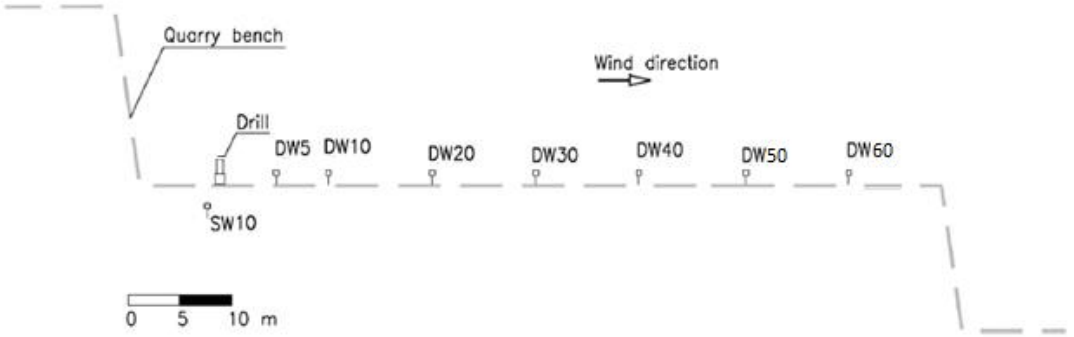

Figure 17: Schematic presentation of the measurement set up. modified from: Sairanen and Selonen (2017)

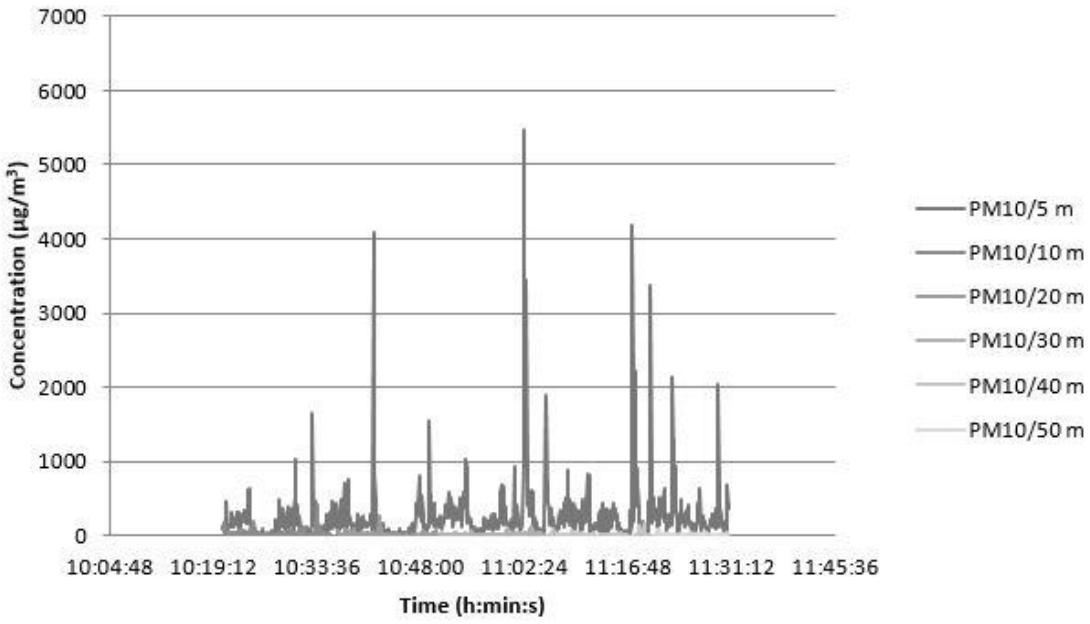

Figure 18: Overview of the PM_{10} observed data at 28/02/2013 source: Sairanen & Selonen (2017)

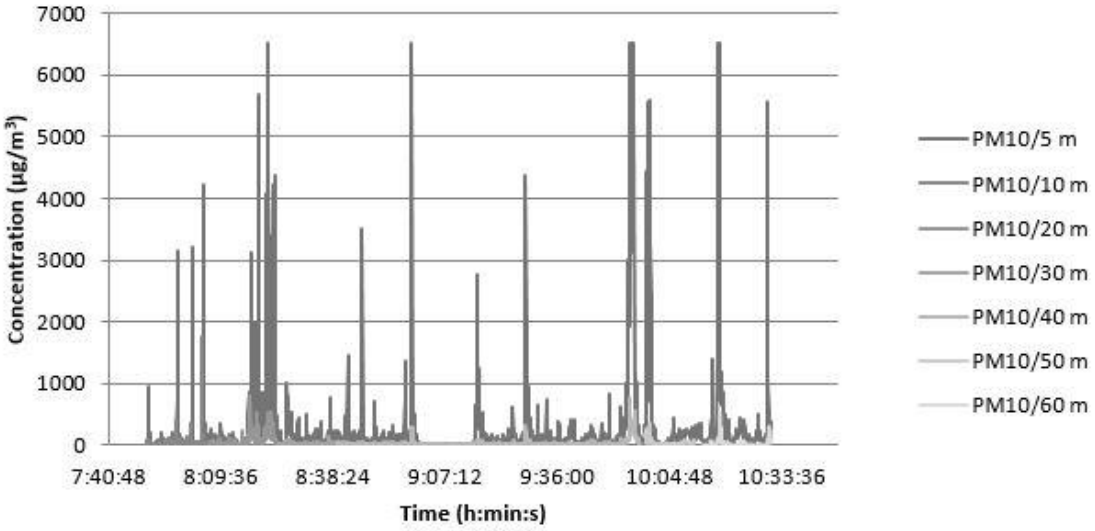

Figure 19: Overview of the PM_{10} observed data at 01/03/2013 source: Sairanen & Selonen (2017)

The frequency of the concentration of the observed data is shown for both days in Figure 20 together with percentile Table 7. The figures show the frequency of the concentration for different concentration bins. The cumulative percentage line shows the percentage at each interval of the frequency distribution. In Figure 21 and Figure 22 is the observed data shown for the separated days with Table 8 and Table 9 as the percentile tables. For 01/03/2013 in Figure 22 it gives a higher frequency of lower concentrations in the observed data than 28/02/2013 in Figure 21.

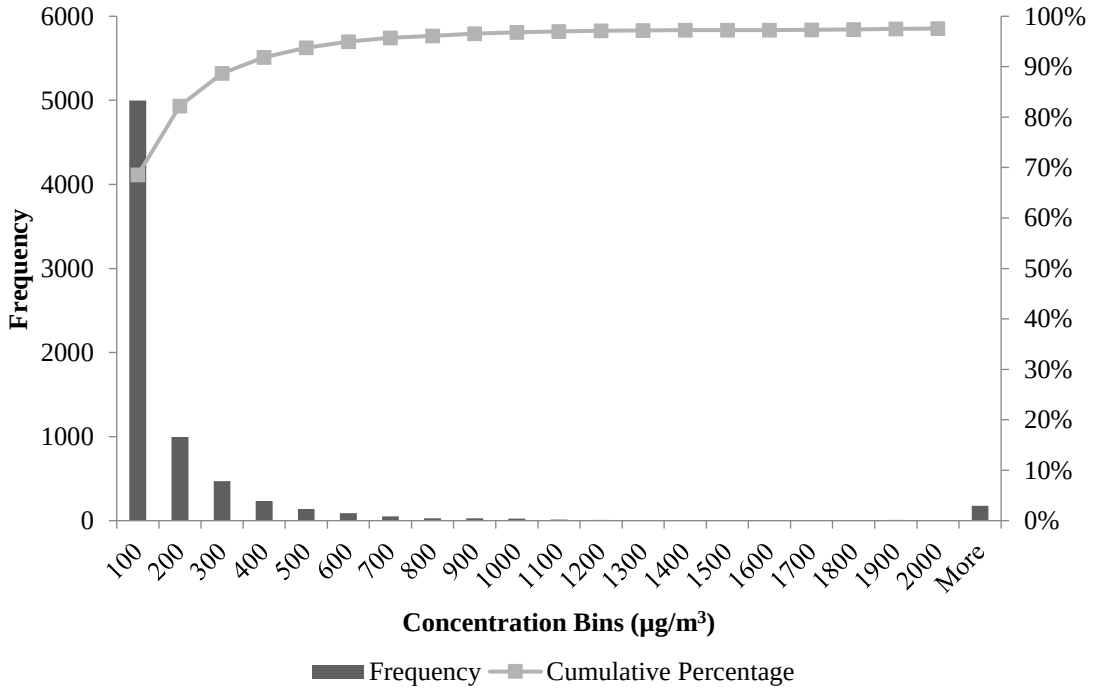

Figure 20: Analyze of the observed data for both days

Table 7: Analyze of the observed data for both days with percentile and concentration of Figure 20

Percentile	**µg/m^3**
50th	44
60th	67
70th	107
80th	177
90th	336
95th	600
98th	2437
99.9th	6528
Max	6528

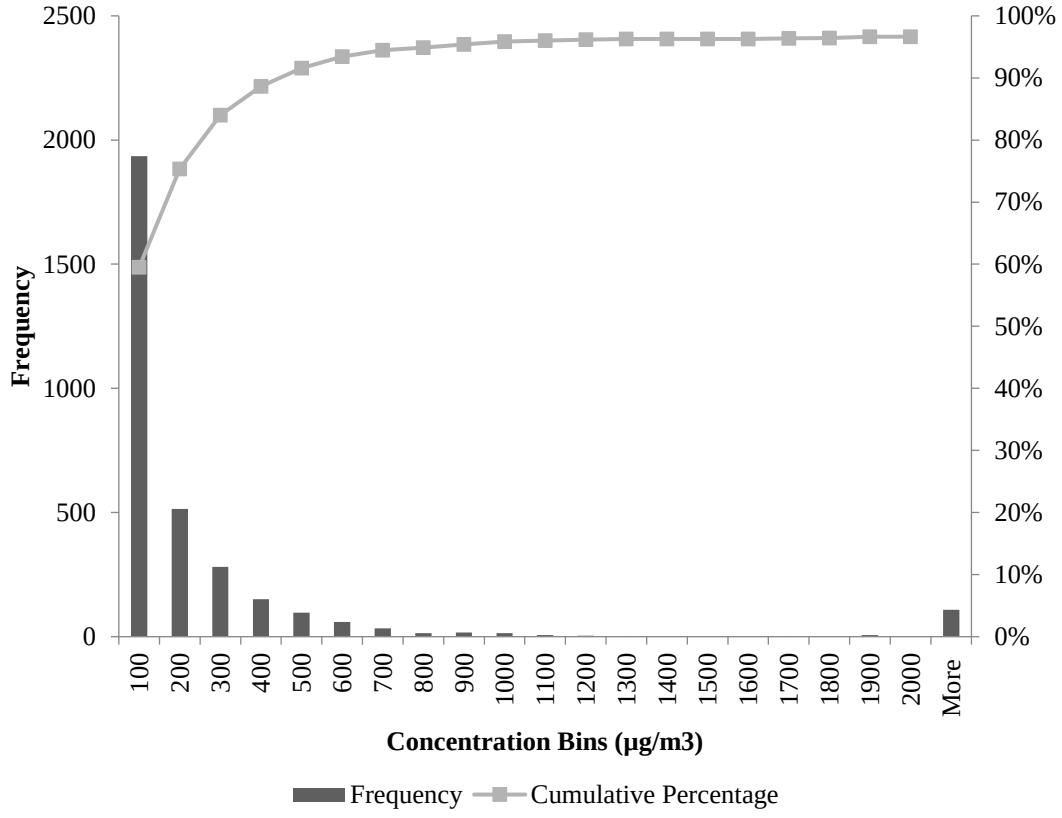

Figure 21: Analyze of the observed data for 28/02/2013

Table 8: Analyze of the observed data for 28/02/2013 with percentile and concentration of Figure 21

Percentile	**µg/m^3**
50th	65
60th	103
70th	155
80th	244
90th	432
95th	822
98th	4176
99.9th	6528
Max	6528

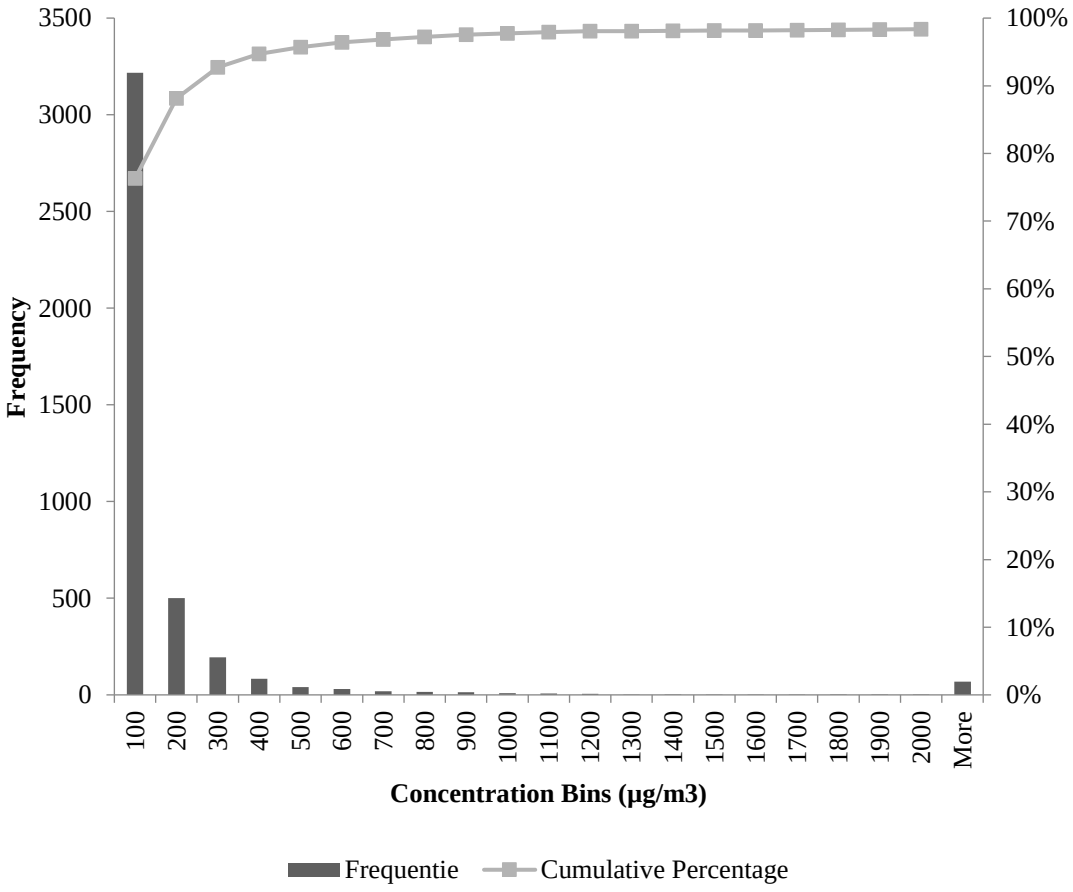

Figure 22: Analyze of the observed data for 01/03/2013

Table 9: Analyze of the observed data for 01/03/2013 with percentile and concentration of Figure 22

Percentile	**µg/m^3**
50th	32
60th	48
70th	74
80th	120
90th	228
95th	431
98th	1165
99.9th	6528
Max	6528

The concentration of the observed data is shown in the decay curve in Figure 23. The background concentration of the decay curve is 8 µg/m^3. According to the exponential equation 7 the decay curve achieves the background concentration at 83 meters.

$$C_{PM_{10}} = 173e^{-0.037x} \quad (7)$$

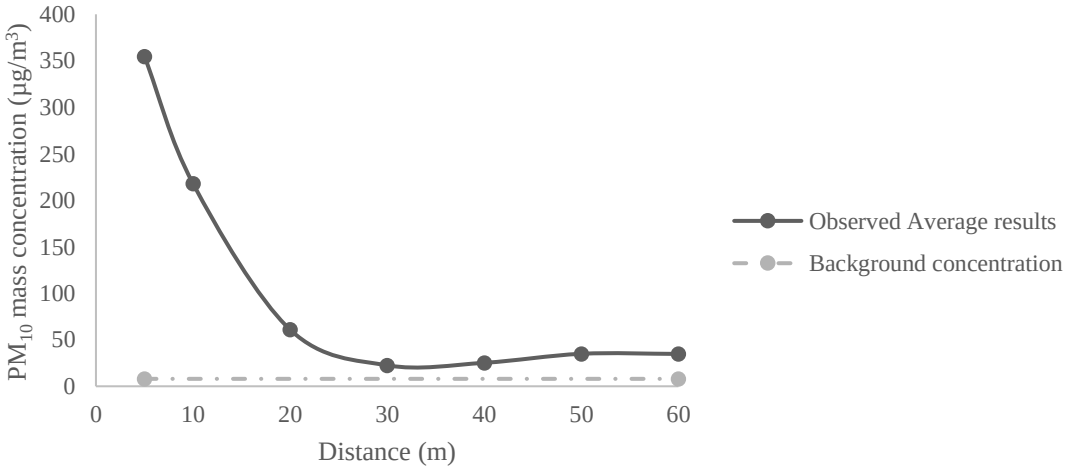

Figure 23: Decay curve of the observed data for both days

3.3 Case study models

The different case studies are developed to evaluate the performance of the model. The different parameters for the case studies are explained in 3.4. The source and receptors are shown in Figure 24. As shown in the figure the receptors are in line with the source and at the same elevation. With the labels R5, R10, R20, R30, R40, R50, R60 and SW10.

The labels are created that the R represents receptor and 5 for 5 meter distance from the source. The SW label is south west from the drilling point. In case study 1 is chosen as a basic elevation model. It is created to have a good comparison with the other case studies. The model is at the actual elevation, source and receptors of the quarry.

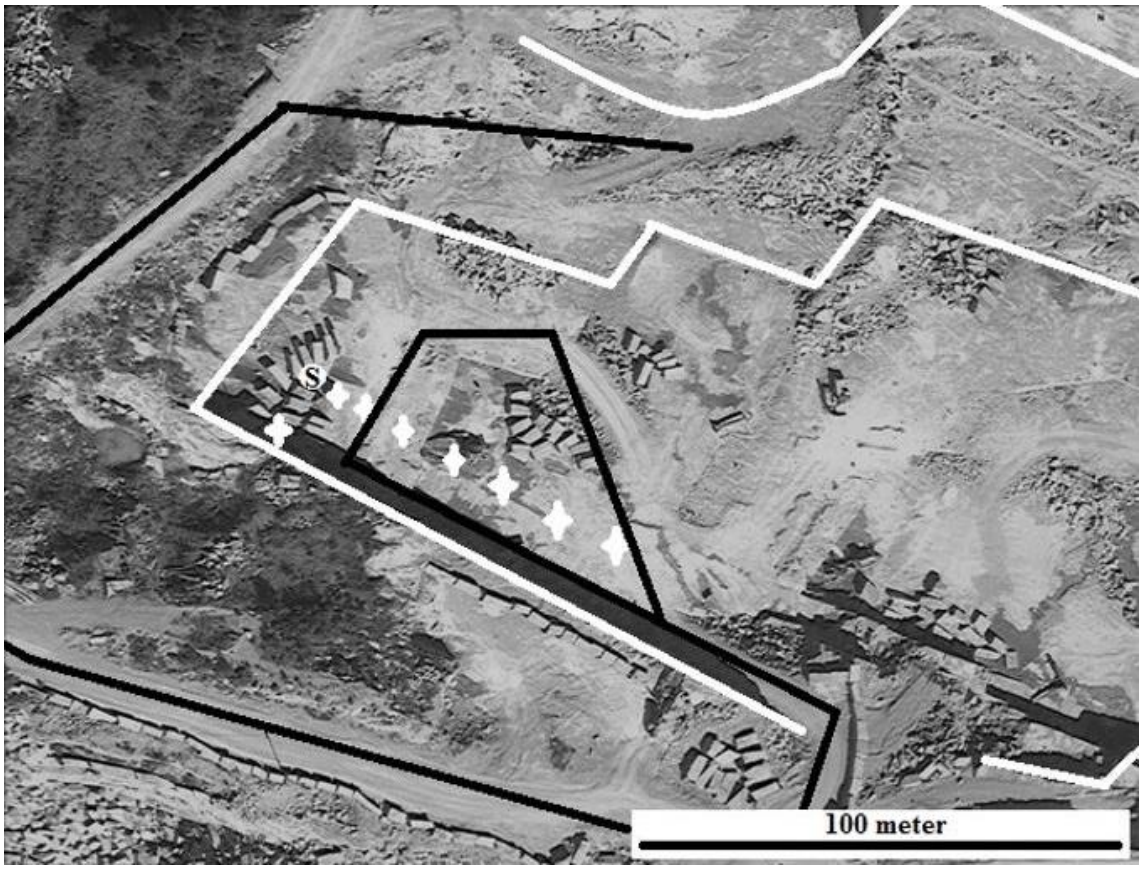

Figure 24: Overview of white stars are the source (S) and receptor points (R5, R10, R20, R30, R40, R50, R60 and SW10) in the quarry. The white lines indicate the quarry walls and black lines the haul roads

3.4 Emission estimation

The emission estimation is dependent of parameters such as meteorological, topographic conditions and the material characteristics. The amount of emission rate for the operation or source on site into the atmosphere need to be calculated. This emission factors will be an estimation and inserted to the discharging points in the given area. It includes all the operations that where active during the observed period. In this chapter will the different dust sources explained. The case studies will be explained together with which dust emission factors of the sources.

3.4.1 Drilling source

The drilling source is most representative for a point source and is inserted in all of the case studies. The source point is explained in detail in Table 2. This is an emission with a very small opening such as a stack or vent. (EPA, 2016) This small opening is representing the drilling rig of the drilling machine. The drilling emission is calculated with the equation of Chakraborty, et al. (2002) and shown in equation 8.

$$E = 0.0325[(100 - m) * su\{(100 - s)m\}^{-1}]^{0,1}(df)^{0.3} \quad (8)$$

Where E = emission rate (g/s)

m = moisture content (%)

s = silt content (%)

u = wind speed (m/s)

d = hole diameter (mm)

f = frequency (number of holes)

In equation 8 the wind speed is changing for every hour according to the meteorological data. The emission factor is calculated hourly and inserted in the model for the measurement days. The other parameters to calculate the emission rate for the drilling source are shown in Table 10.

Table 10: Overview of the parameters source: Sairanen & Selonen (2017) and GTK (2017)

Activity	**Source type**	**Parameters**	**Values**	
Drilling	Point	Moisture content	0.12	%
		Silt content and cuttings	36	%
		hole diameter	30	mm
		Frequency of drilling	3	Number of holes/day
		Production a day	6.85	m^3
		Drilling capacity	0.14	m/s

3.4.2 Haul roads and waste dump

Case study 2 is an addition to the case study 1. In case 2 the haulage roads, buildings and waste dump are added into the model. Case 2 is to estimate the performance of the model to take the other activity in the quarry into account. To calculate the emission factor for the haul roads the equation 9 is used from the literature Chaulya, (2006). The information for equation 9 is shown in Table 10 and Table 11 . For haul roads the most representative dust source is assumed to be a volume source just above the ground surface.

$$E = [\{(100 - m)m^{-1}\}^{0.35} * \{(us)(100 - s)^{-1}\}]^{0,7}\{0.5 + 0.1(f + 0.42v)\}10^{-3} \quad (9)$$

Where E = emission rate (g/s)

m = moisture content (%)

s = silt content (%)

u = wind speed (m/s)

f = frequency of loading (no. h^{-1})

v = average vehicle speed (m/s)

Furthermore, the waste dump is added as equation 10 in an area source. The equation is from the literature Chakraborty, et al., (2002). The Table 12 is the additional information needed for the waste dump equation. In Table 12 the factors for the buildings are given.

$$E = [\{(100 - m)(m)^{-1}\}^{0.2}\{(s)(100 - s)^{-1}\}^{0.1}\{(u)(2.6 + 120u)^{-1}\}\{(a)(0.2 + 276.5a)^{-1}\}] \quad (10)$$

Where E = emission rate (g/s)

m = moisture content (%)

s = silt content (%)

a = area (km^2)

Table 11: Overview parameters for equation 10 and 11 source: Sairanen & Selonen (2017) and Google Earth 2015

Activity	Source type	Parameters	Values	
Haul road	Volume	Frequency of loading	1	No. $*h^{-1}$
		Average of vehicle speed	8.333	m/s
Waste dump	Area	Area	0.0216	km^2
Building 1	Rectangle	Volume	0.840	km^3
Building 2	Rectangle	Volume	0.192	km^3

3.4.3 Open pit

The open pit source equation is used to create case study 3. It is an addition of the case study 2 open pit estimation with the equation 11 and Table 12. Equation 11 is from the literature of Chaulya, (2006). The open pit estimation is another tool than the area source in AERMOD. (Neshuku, 2012) It considers a dust source all over the quarry area. The open pit source is used with all the normal elevation and emission factors from case 2 where used. The open pit source is tested to see if the dust sources need an additional component of dust source from the whole quarry.

$$E = [\{(100 - m)(m)^{-1}\}^{0.1}\{s(100 - s)^{-1}\}^{0.3}a^{1.6}\{(u)(10 + 125u)^{-1}\}] \quad (11)$$

Where E = emission rate ($g/s*m^2$)

s = silt content (%)

u = wind speed (m/s)

a = area (km^2)

m = moisture content (%)

Table 12: Overview parameters for equation 11 source: Google Earth 2015

Activity	Source type	Parameters	Values	
Open pit	Open pit	Area	0.05070	km^2

3.4.4 Surface Roughness

Case 4 is an addition of Case 2 with the surface roughness set to 0.300. The parameter is used as the quarry or mine factor in AERSURFACE User Guide, (2013). The parameter is a seasonal surface roughness parameter. It is an estimation reflecting the significant surface expression (EPA, 2013).

Part IV: Results

4.1 Emission rates

As discussed in the modeling chapter, an emission inventory was compiled from the different sources of PM_{10} at the quarry Taivassalo. The results from the emission estimation are discussed in the following sections. The calculated emission factors according to the equations from part III are gathered in Table 13. The different activities gives different rates of PM_{10}.

Table 13: Emission rates calculated in part III for PM_{10}

		Average emission rate		
Source		**28/02/2013**	**01/03/2013**	**Used in Case study**
Drilling machine	(g/s)	0.264	0.270	1,2,3 and 4
Haul road	(g/s)	0.008	0.009	2,3 and 4
Waste Dump	(g/s)	0.182	0.183	2,3 and 4
Open pit	(g/s*m^2)	0.012	0.012	3

For every hour the emission rate changes due to the sources in the model. The drilling emission has the highest value. The activity in the quarry will give difference in the emission rate at various locations. The haul road is the activity of handling the material from loading to unloading point. The waste dump is located in the quarry area roughly 30 meters from the drilling source. The waste dump does not act as unloading point for the mining activity.

4.2 Meteorological summary

The wind rose gives a predominant wind directions recorded during study period were the west-northerly and north-easterly. An overview if both days is shown in Figure 25: Wind rose on 28/02/2013 between 11:00-13:00 (left) and on 01/03/2013 between 07:00-11:00 (right). The wind speed has a range of 3.09 m/s to 5.14 m/s with an average of 4.20 m/s. In the modeling process there is no wind speed below 1 m/s recorded. The ambient temperature experienced was from 0.85 ºC to 4.85 ºC. A total hourly overview of the observed meteorological data and wind roses are displayed in appendix B.

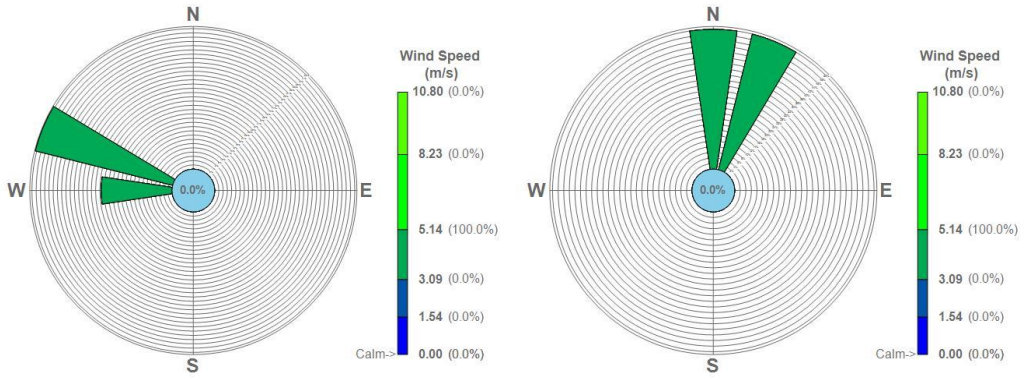

Figure 25: Wind rose on 28/02/2013 between 11:00-13:00 (left) and on 01/03/2013 between 07:00-11:00 (right)

4.3 Performance measurements

4.3.1 Model performance

The different performance of the observed and modelled data is evaluated with the mean, standard deviation, minimum, maximum and median of the dust concentration. The values are displayed in Table 14 and Table 15. AERMOD gives high results compared with the observed data. In case study 1 gives a minimum of 0 µg/m^3. This means that there was no predicted dust particles during that time. Case study 3 is not shown because it gives identical outcome of case study 2. Therefore, results only for case studies 1, 2 and 4 are presented hereafter. The raw data of the receptor points are presented in Appendix C. Spread of the all the data points is shown in Figure 26 and Figure 27 as Box and Whisker plots. The line caps are presenting the minimum and maximum concentration. The median in the box is the skewed line.

Table 14: AERMOD model performance assessment for 28/02/2013

	MEAN	**STDEV**	**MIN**	**MAX**	**MED**
Observed	207	237	18	742	127
Case study 1	4,015	4,692	0	12,578	1,972
Case study 2	4,182	4,609	68	12,650	2,144
Case study 4	4,012	4,426	67	12,058	2,060

Table 15: AERMOD model performance assessment for 01/03/2013

	MEAN	**STDEV**	**MIN**	**MAX**	**MED**
Observed	115	119	23	326	76
Case study 1	4,760	5,728	0	1,2890	997
Case study 2	519	651	141	2,388	234
Case study 4	497	740	117	2,846	227

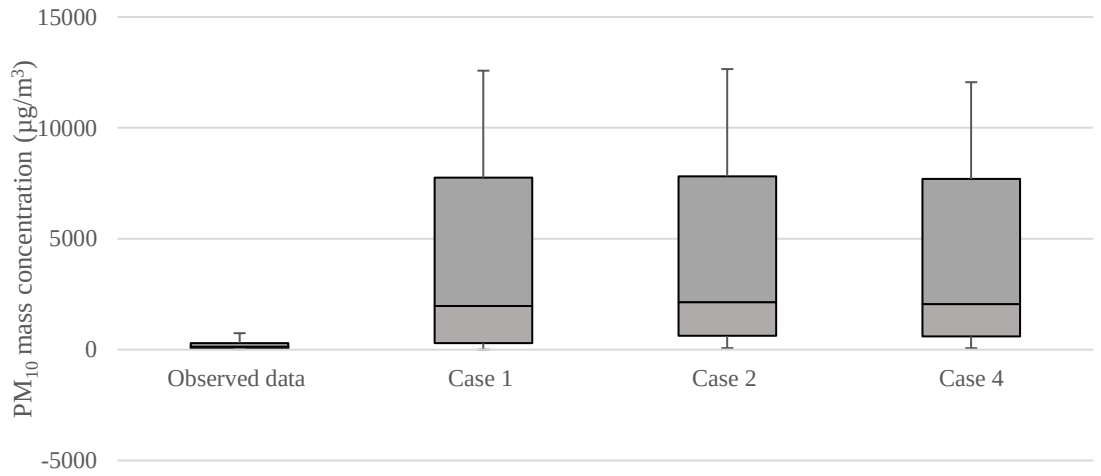

Figure 26: Box and Whisker plot for 28/02/2013 observed data and case studies 1, 2 and 4

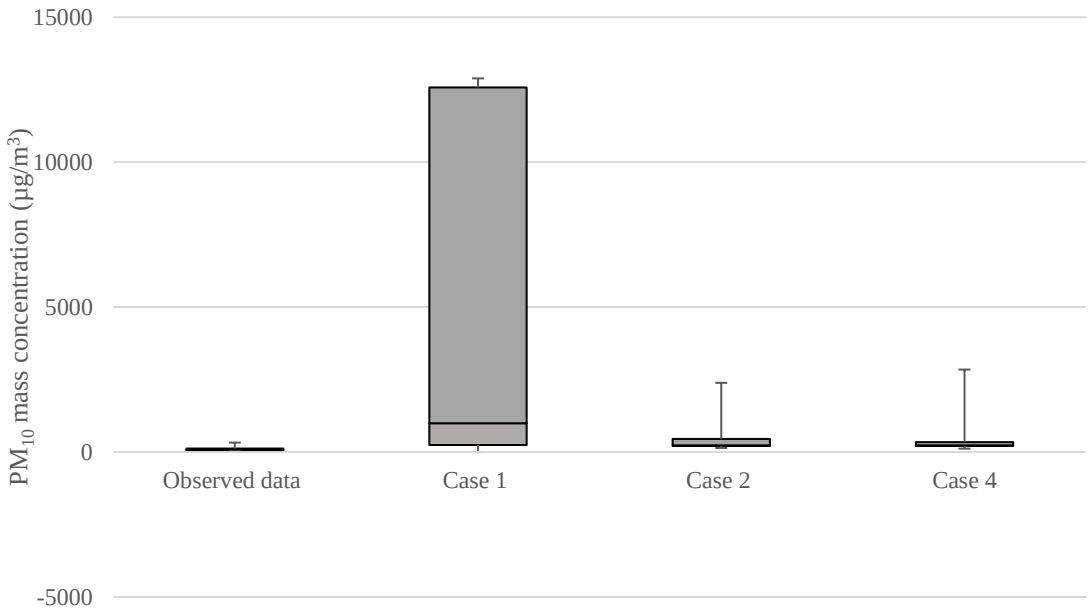

Figure 27: Box and Whisker plot of 01/03/2013 observed study and case studies 1, 2 and 4

The performance measurements are shown in Table 16 and Table 21 with the fractional bias (FB), geometric mean bias (MG), normalized mean squared error (NMSE) and fraction of data satisfying the expression (FAC2). As described before these values are calculated with equation 5-9 in chapter 2.3.3 model performance assessment.

In Table 16 and Table 17 are all the receptor points shown. The outcome of case 1 is specified for the hour and place. The receptors with an output of 0 µg/m^3 have an NA in the tables.

Table 16: Overview of performance assessment 28/02/2013 in case 1

		FB	**MG**	**NMSE**	**FAC2**
10:00-11:00	**R5**	-1.93	0.02	56.3	58
	R10	-1.96	0.01	107.3	109
	R20	-1.91	0.02	39.5	41
	R30	-1.84	0.04	22.8	25
	R40	-1.73	0.07	12.0	14
11:00-12:00	**R5**	-1.69	0.08	10.1	12
	R10	-1.68	0.09	9.6	12
	R50	-0.88	0.39	1.0	3
12:00-13:00	**R5**	-1.88	0.03	29.6	32
	SW10	NA	NA	NA	NA

Table 17: Overview of performance assessment 01/03/2013 in case 1

		FB	MG	NMSE	FAC2
07:00-08:00	**R5**	-1.98	0.01	164.5	166
	R10	-1.97	0.01	120.7	123
	SW10	NA	NA	NA	NA
08:00-09:00	**R5**	-1.90	0.03	37.5	40
	R10	-1.93	0.02	55.6	58
	R20	-1.67	0.09	9.2	11
	R30	-1.81	0.05	18.1	20
	R40	-1.64	0.1	8.3	10
09:00-10:00	**R5**	-1.90	0.03	36.6	39
	R40	-1.60	0.11	7.0	9
10:00-11:00	**R5**	-1.91	0.02	39.9	42
	R50	-1.32	0.21	3.1	5
	R60	-1.01	0.33	1.4	3

In Table 18 and Table 19 are all the receptor points shown. The outcome of case 2 is specified for the hour and place.

Table 18: Overview of performance assessment 28/02/2013 in case 2

		FB	MG	NMSE	FAC2
10:00-11:00	**R5**	-1.93	0.02	56.7	59
	R10	-1.96	0.01	108.9	111
	R20	-1.93	0.02	51.6	54
	R30	-1.91	0.02	40.7	43
	R40	-1.88	0.03	30.6	33
11:00-12:00	**R5**	-1.69	0.08	10.2	12
	R10	-1.69	0.08	9.9	12
	R50	-1.68	0.09	9.5	11
12:00-13:00	**R5**	-1.88	0.03	29.8	32
	SW10	1.43	6.07	4.2	0.2

Table 19: Overview of performance assessment 01/03/2013 in case 2

		FB	MG	NMSE	FAC2
07:00-08:00	**R5**	-0.71	0.48	0.6	2
	R10	-1.46	0.16	4.6	6
	SW10	-1.81	0.05	17.8	20
08:00-09:00	**R5**	-0.57	0.56	0.4	2
	R10	-1.42	0.17	4.1	6
	R20	-1.13	0.28	1.9	4
	R30	-1.65	0.10	8.5	10
	R40	-1.58	0.12	6.7	8
09:00-10:00	**R5**	-1.23	0.24	2.5	4
	R40	-1.54	0.13	5.8	8
10:00-11:00	**R5**	0.72	2.14	0.6	0.7
	R50	-1.42	0.17	4.1	6
	R60	-1.53	0.13	5.6	7

The modelled results of case 3 are identical to case study 2. Therefore the results of case 3 are not being displayed. The open pit source did not have any influence on the modelled results.

The results of case study 4 are presented in Table 20 and Table 21. The outcome is showed for every receptor per hour and place.

Table 20: Overview of performance assessment 28/02/2013 in case 4

		FB	MG	NMSE	FAC2
10:00-11:00	**R5**	-1.93	0.02	53.9	56
	R10	-1.96	0.01	101.2	103
	R20	-1.92	0.02	48.6	51
	R30	-1.90	0.02	38.9	41
	R40	-1.88	0.03	29.5	31
11:00-12:00	**R5**	-1.69	0.08	10.1	12
	R10	-1.68	0.09	9.5	11
	R50	-1.67	0.09	9.3	11
12:00-13:00	**R5**	-1.87	0.03	28.2	30
	SW10	1.44	6.18	4.3	0.2

Table 21: Overview of performance assessment 01/03/2013 in case 4

		FB	MG	NMSE	FAC2
07:00-08:00	**R5**	-0.49	0.61	0.3	2
	R10	-1.44	0.16	4.3	6
	SW10	-1.84	0.04	21.6	24
08:00-09:00	**R5**	-0.18	0.84	0.03	1
	R10	-1.28	0.22	2.8	5
	R20	-1.09	0.29	1.7	3
	R30	-1.64	0.10	8.2	10
	R40	-1.57	0.12	6.5	8
09:00-10:00	**R5**	-1.01	0.33	1.4	3
	R40	-1.53	0.13	5.6	7
10:00-11:00	**R5**	0.88	2.57	1.0	0.4
	R50	-1.44	0.16	4.3	6
	R60	-1.56	0.12	6.2	8

4.3.2 Sensitivity analyses

The sensitivity analyses is only done for case 2. Case study 2 is most fitting with the observed data as shown in chapter 4.3.1 model performance. The sensitivity analyses are done to see how it influences case study 2 when parameters are being changed. In appendix D is shown in which range the parameters are changed for the sensitivity analyses. The Albedo has a range of 0.06 until 2.00. For the Bowen ratio has a range of 0.14 until 1.14. The Monin-Obukov length has a range -1,366 m until 1,386 m. It is only negative for 28/02/2013 and positive for the first three hours. For the surface roughness it ranges from 0.057 m until 0.858 m. Emission Factor has a range of 0.013 until 0.546 g/s. The wind speed is in a range of 1 m/s until 11 m/s. The wind speed is not allowed to be lower than 1 m/s. (EPA, 1995). In appendix E are the figures for the sensitivity analyses shown for a specific hour of both observed days. The most observed data is collected during these days. The figures show that the emission factor has a great influence on the model. The emission factor is shown specific per receptor in Figure 28 and Figure 29. In these figures the observed data is displaced to compare it with the modelled output.

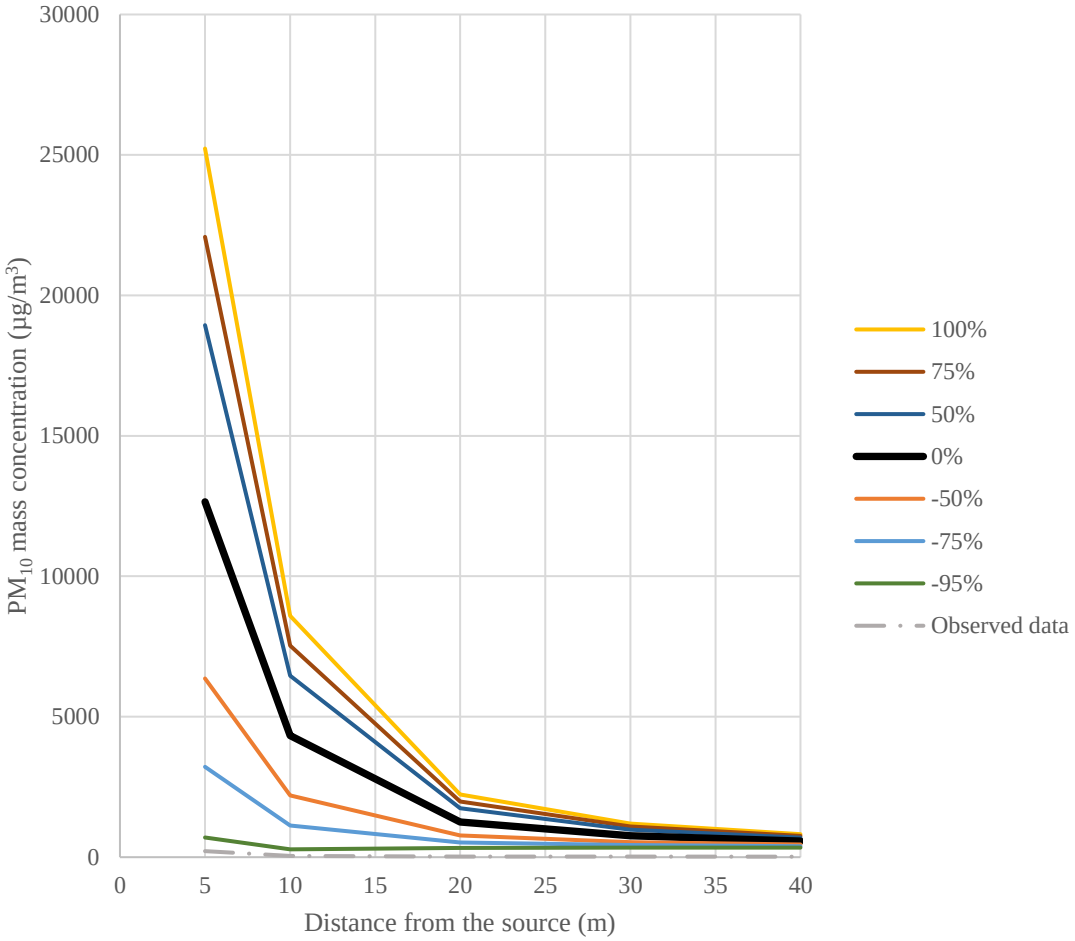

Figure 28: Sensitivity analyses 28/02/2013 case 2 for emission factor and the observed data

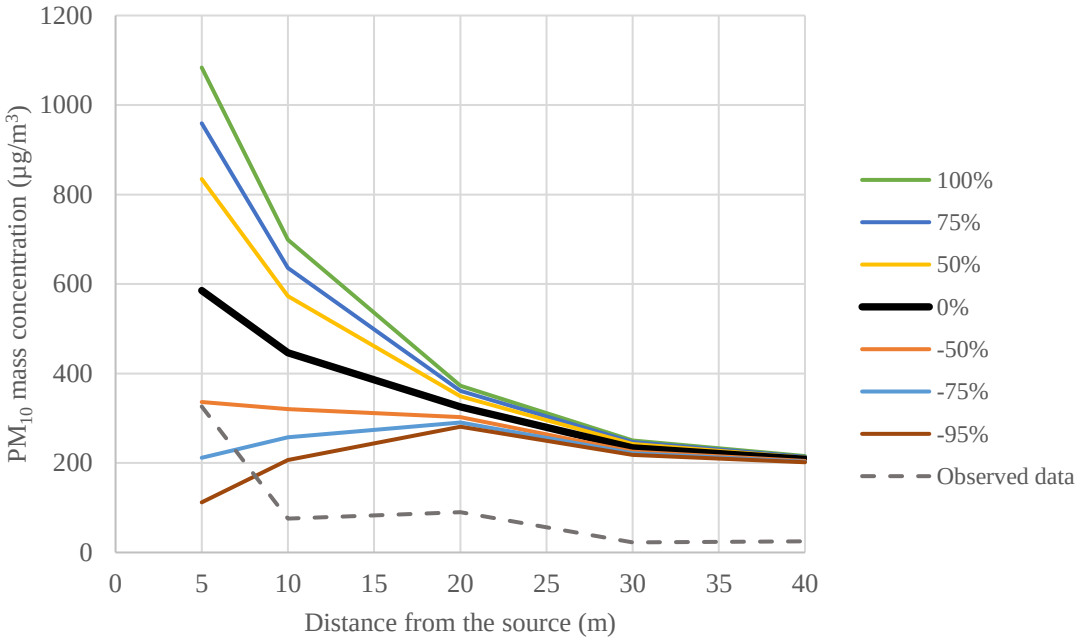

Figure 29: Sensitivity analyses 01/03/2013 case 2 for emission factor and the observed data

4.3.3 Validation curve

The validation curves are shown for the case studies 1, 2 and 4. The validation curves are reflecting the observed data on the x axis and the predicted data on the y axis. The validation curves are shown for case 2 in Figure 30 and Figure 31. The other cases are presented in Appendix F. All the figures have the line with a slope 1:1 line to indicate a good fit model. (Zou, et al., 2010) The validation curve for case 2 has an underprediction with 53.3 percentile for 28/02/2013. The underprediction is for the receptor point SW10. The validation curve for case 2 has an underprediction with 91.1 percentile for 01/03/2013.

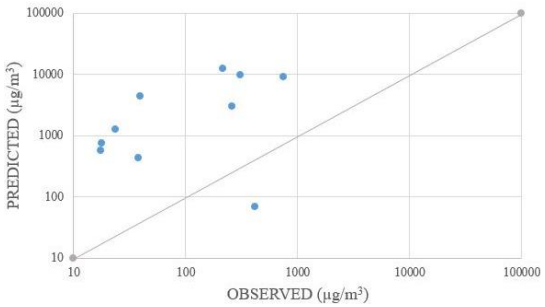

Figure 30: Q-Q plot 28/02/2013 for observed and case 2

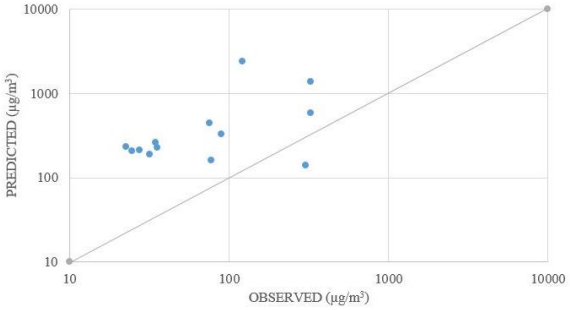

Figure 31: Q-Q plot 01/03/2013 for observed and case 2

4.3.4 Decay curve

A decay curve shows how the dust concentration varies in distance for all the predicted data. All the data is inserted in the graph to compare it with the observed decay curve in in Figure 23. In Figure 23 and Figure 32 are the background concentration line of 8 µg/m^3 inserted from the literature Sairanen, (2017). The decay curve in Figure 32 shows an exponential equation 12. The result of equation 12 gives together with the given background concentration from Sairanen (2017) is achieved at 127 meters for case 2. Both the decay curves of Figure 23 and Figure 32 show a decrease in dust concentration with decreasing distances.

$$C_{PM_{10}} = 3{,}000e^{-0.047x} \quad (12)$$

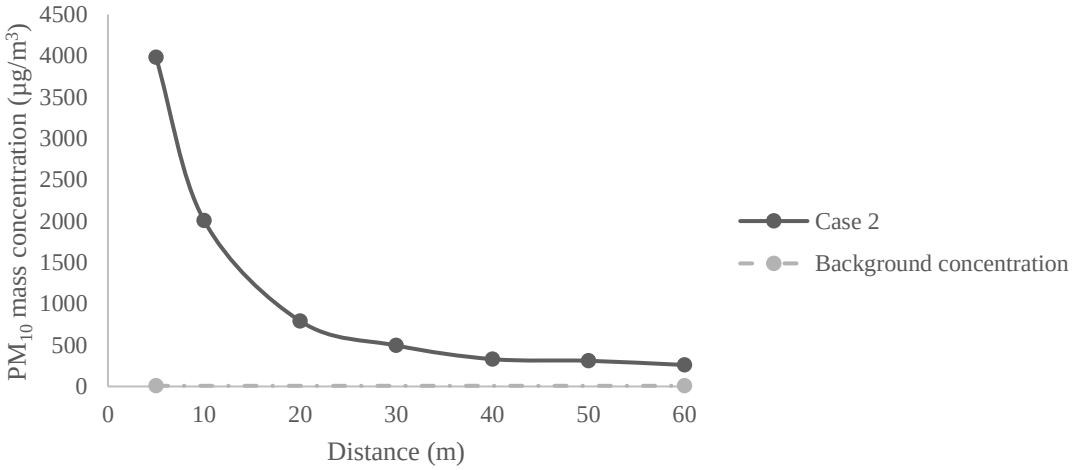

Figure 32: Decay curve of all the predicted data and the background concentration

4.3.5 Analyst figures

The figures are created for case 2 to have an indication how the dust concentration is spreading in the area of the quarry. The figures show the North Easting coordinates and legend with the color ranges of PM_{10} concentration in µg/m^3. The software Analyst is used to create the dust dispersion figures. From Figure 33 until Figure 35 it is shown for the day 28/02/2013. The Figure 36 until Figure 38 is shown for 01/03/2013. Appendix G shows an overview of the dust dispersion for both days with hourly dispersion spread for changing emission factor.

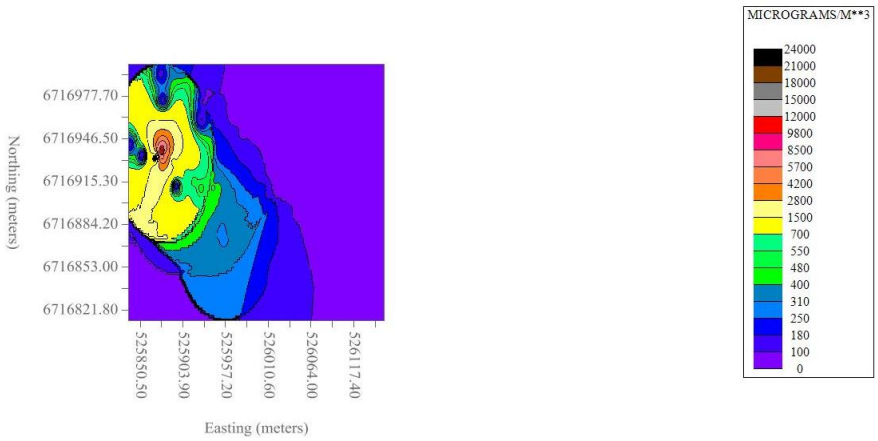

Figure 33: Dust dispersion at 28/02/2013 between 10:00-11:00

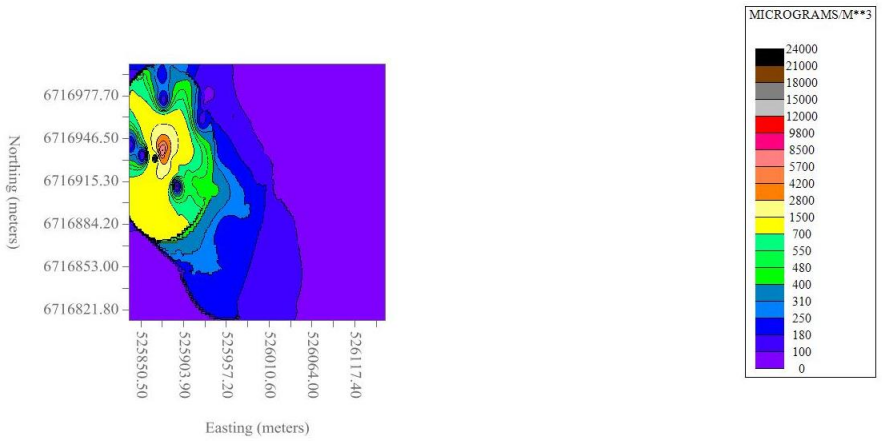

Figure 34: Dust dispersion at 28/02/2013 between 11:00-12:00

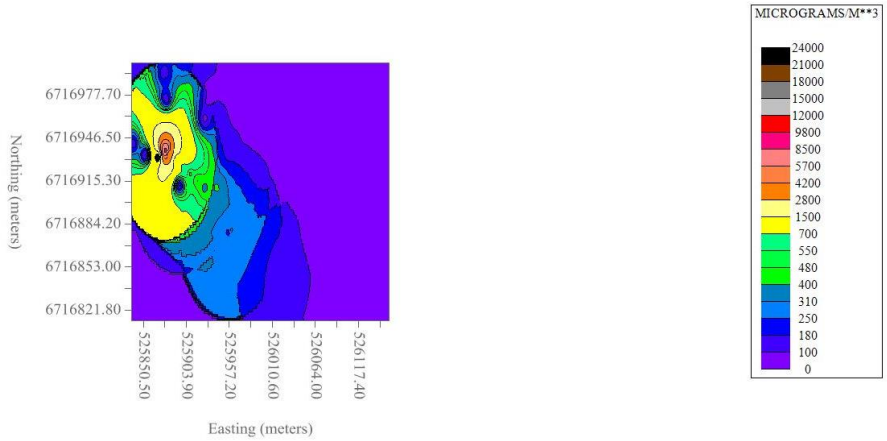

Figure 35: Dust dispersion at 28/02/2013 between 12:00-13:00

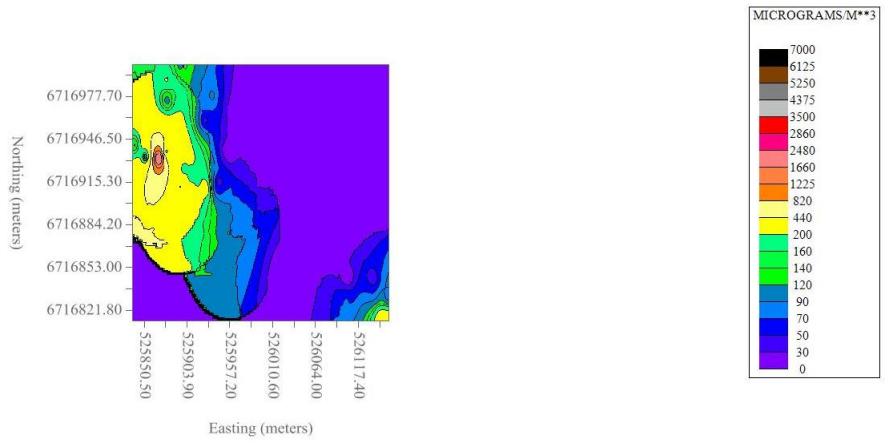

Figure 36: Dust dispersion at 01/03/2013 between 07:00-08:00

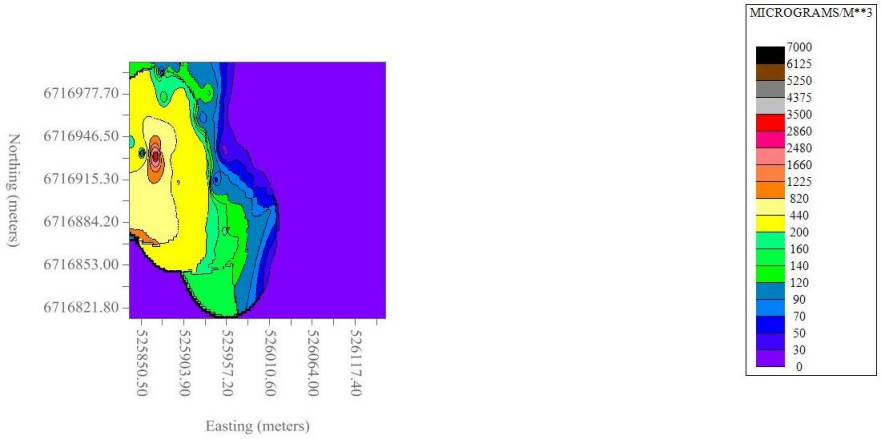

Figure 37: Dust dispersion at 01/03/2013 between 08:00-09:00

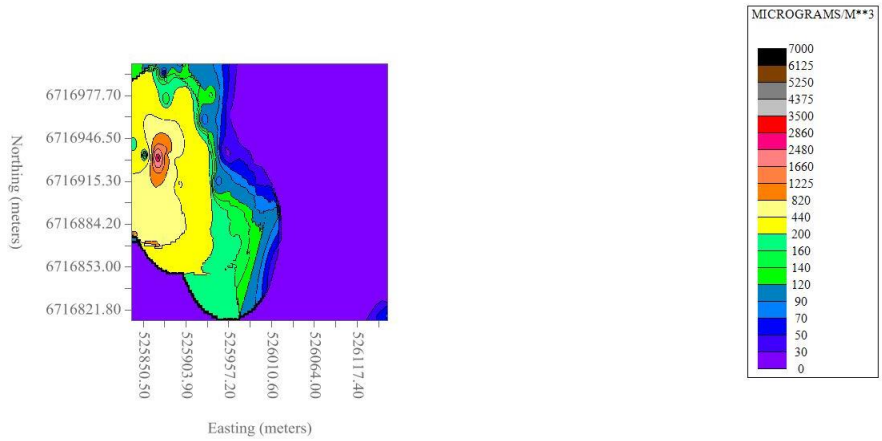

Figure 38: Dust dispersion at 01/03/2013 between 10:00-11:00

Part V: Discussion

The receptor points are chosen to be aligned downwind and at one straight line with the drilling source. The chosen location of these receptor points is not indicated with exact GPS data. The receptor SW10 is located at the other side of the drilling source. This will create a variation in the predicted data. The receptor point is located between the steep wall and the drilling source. For SW10 it could be considered that the wind will behave turbulence instead of the Gaussian plume. It has a lower overprediction than the other receptors.

During each measurement day there was a different wind direction. The effect of dominated east wind on 28/02/2013 and north wind for 01/03/2013 indicates an effect on the Gaussian dispersion plume. The receptor points are aligned in South-East from the drilling source as has been shown in Figure 11. In Appendix B, the meteorological data shows that all the different weather parameters are in the same range for 01/03/2013, except for Monin-Obukov Length between 10:00-11:00. The data of 28/03/2013 shows a higher deviation for every parameter. Except for the Bowen Ratio parameter, that is not changing. It can be further discussed whether the initial wind direction of the day has a further influence on the concentration.

The box and whisker plots in Figure 26 and Figure 27 give information about the statistical distribution of the observed and predicted data. The spacing between the different parts of the box indicate the dispersion (spread) (Dekking, et al., 2005). The dispersion of the data is high for both days for case 1. Half of the data points are less than the median line. The first quartile is small for all the case studies. The median is actually closer to the minimum than the maximum. The median is closer to the first quartile and the bottom whisker than the upper whisker. The highest upper whisker can be seen for case 2 and 4. The upper tail is longer and indicates a positive skewness. The positive skewness means a distribution shape of right-leaning curve. It does not apply for case 1, because the zero point balances on both sides out overall.

Table 14 and Table 15 also show the relationship between the median and the mean concentration. The relationship is that the median is lower than the mean of the concentrations for all the case studies. The difference of the standard deviation of the case studies will indicate how the concentration spreads around the center. For case 2, the standard deviation of the concentration is the best comparable with the observed data from 01/03/2013. However, still all cases show a concentration which is higher than the observed data.

The results of the performance assessment model for case 1 indicate that the model is not applicable (NA). Therefore, the results of case 1 are not required to discuss further, because the equations do not allow a concentration of zero. The under estimation of case 1 is probably due to the fact that there was no PM_{10} background concentration level inserted in AERMOD.

The performance model assessment shows for FB that observed and predicted data is matching. The results of the FB for the compared data would give negative values and for a perfect model it would give a value of zero. For case 2 and 4 it gives a positive outcome for two receptor points. The receptor points, SW10 at 28/02/2013 between 12:00-13:00 and R5 at 01/03/2013 between 10:00-11:00, have a lower predicted concentration than the observed concentration. The FAC2 shows the same results as the

FB. Only the MG is to be considered together with FB. It is considered as a good model if the MG gives a 1. Both receptor points of a positive FB give not a good result for MG. This implies a negative performance for the PM_{10} analyze at these receptor points, SW10 and R5, compared with the other receptor points. If the receptor points distance from the drilling source are compared, it gives a higher overprediction. A FB of -0.67 is an equivalent of an overprediction of a factor 2 (Chang & Hanna, 2004). Comparing the receptor points by their place of the distance from the drilling source. It gives a higher overprediction for the receptor points further away from the drilling source. NMSE implies during 28/02/2013 another outcome than during 01/03/2013. It is shown that the closer receptor points do not have a normal distribution. For 01/03/2013 the NMSE has a much better normal distribution.

The sensitivity analyses show that the model case 2 is done for six parameters. Case 2 was not sensitive for the Bowen Ratio, Albedo and wind speed parameters. The most important parameters are firstly emission factor, secondly surface roughness and thirdly Monin-Obukov length. An obvious result is that the emission factor has the highest impact for the sensitivity analyses. Figure 28 and Figure 29 show a correlation between the observed and the predicted data with changing emission factor. At R20 the sensitivity lines of PM_{10} mass concentration becomes more stable. It means that the emission factor has less impact when the receptor point is further away from the drilling source. Figure 28 for 28/02/2013 has a fit curve with the observed data for the lowest emission factor -95% (0.013 g/s). Figure 29 for 01/03/2013 shows for the different emission factors the -75% and -95% are not correlating and is lower than the observed data. During 01/03/2013, would the emission factor of -50% (0.132 g/s) be as a represented fit with the observed data. In Appendix E, for E_11 and E_14 shows that the correlation of the observed data and predicted data is less correlated on 28/02/2013 as on 01/03/2013. The surface roughness and Monin-Obukov length have less influence on the PM_{10} mass concentration for 28/02/2013 than on 01/03/2013. The surface roughness parameter has influence when it goes into a different value, because AERMOD has different categories for landcover of the surface roughness. The Monin-Obukov shows to be most stable for the PM_{10} concentration, because it has positive values for the meteorological data. Both Surface Roughness and Monin-Obukov length show less deviation of the PM_{10} mass concentration when the receptor point is further away from the drilling source.

With validation curves it was possible to evaluate the model. The Q-Q plots showed all hourly predictions for both days. For all case studies, the plots show a high overprediction. The percentile is higher for 01/03/2013, because at 28/02/2013 it has the outlier SW10. If we neglect the SW10 concentration then the percentile will be 98.8 for case 2 at 28/02/2013 instead of 53.3 percentile. The percentile is in better accordance with this value, from where the outlier is neglected.

The dust decay curve shows the PM_{10} concentration for the locations of the receptor points. Also shows a correlation between the observed and predicted data. The exponential equations 7 and 12 of the decay curves have a different exponential growth. The parameter of the exponential equation 12 is larger and gives a vertical stretch. The exponential equation 12 shows an overprediction for all receptor points. Another point is that the background concertation was achieved and varied not as much from the observed data. The observed data was achieved at 83 meters and the predicted data at 127 meters.

The Analyst figures are used to indicate how the dust dispersion is spreading in the quarry. It also shows that the dust concentration reaches over the quarry walls. The drilling source

is shown in the Figure 33 until Figure 38 with the highest dust dispersion concentration range. In Figure 33 and Figure 35 it impacts to the west. It confirms the wind direction during those hours for 28/02/2013. The figures also show the impact of the haul roads inserted in case 2. On 01/03/2013, the spread of dust dispersion around the drilling source is higher in the spread North and matches the wind direction. The wind direction shows for the waste dump dust dispersion located roughly 30 meters to the west from the drilling source. Figure 36 has a dust concentration in the south west of the figure. This location is outside the range of the quarry and has no explanation why it is showing the higher dust concentration.

Appendix G shows the sensitivity analyses for the Analyst figures of the different emission factors. The Analyst figures indicate the different spread of the dust concentration from the drilling source. The higher drilling emission gives a high spread of together with the overpredicted results. The model shows nicely that the dust dispersion will travel over the steep walls and further around the quarry area.

Appendix G Figure G_1 until G_7, for 28/02/2013 shows how the dust dispersion spreads with a higher impact for a larger emission factor. Together with the discussion of the sensitivity analyses is the emission factor of -95% (0.013 g/s) a good fit with the observed data. Furthermore, Appendix G Figure G_8 until G_14, for 01/03/2013 show a good spread for the lower emission factors. The low emission factor of -95% is a low dispersion impact and hardly noticeable. When we validate the figures of Appendix G with the sensitivity analyses of Figure 29 -50% (0.132 g/s) of the emission would be a curve fit for the observed case. The emission factors set at -75% and -95% are not correlating and is less than the observed data, because discussed earlier in this chapter. Analyst figures the G_10, with the emission factor of 0.132 g/s is a good representation of dust dispersion for case 2.

Part VI: Conclusion

The objective of this research was to determine if the model can predict the dust dispersion in the near field quarry. The model predicts the average hourly PM_{10} concentration for a distance from 5 meter until 60 meters from the drilling source.

The results of case study 1 are not interesting, because of a concentration of 0.00 $\mu g/m^3$ at receptor point 10 meter for both days.

The AERMOD software gives more reliable results for case study 2. Case study 2 contains more dust emission operations in the model.

The performance assessment gives a reliable distribution of PM_{10} concentration for the receptor points closer to the source. Where the sensibility analyses and decay curve give more stable outcome from further receptor points (>20m).

The investigation for the sensitivity analyses of case 2 show no difference in Bowen ratio, Albedo and wind speed parameters. The model gave altering results for the effects caused by emission factor, surface roughness and Monin-Obukov length.

Validation analyses has an overprediction in the bias. The decay curve shows a clear overprediction. It is shown that the predicted data behavior can validate the observed data and that a good model is obtained.

In conclusion, to answer the research question if the model predicts the dust dispersion in the quarry. The results show a large overprediction during all case studies. The highest overprediction is at the closest receptor of 5 meter. It stabilizes from 20 meters from the drilling machine.

Part VII: Recommendations

The future plans, the AERMOD software can be used to create dust dispersion models for the quarry. There is more data needed for future reference and improvement for creating the model with different emission factors.

In this study an emission inventory of PM_{10} emitted from different types of primary and secondary sources namely drilling source, haul road and waste dump has been made for this quarry. For this study the implementation of different emission sources improved the predicted concentration. A further recommendation for this model Could involve considering different case studies and changes in the variety of dust emissions.

In this study is only looked into one quarry site, it would be interesting to have more sites to evaluate. The quarry site Taivassalo is located in a rural area in a forest area. It was considered that there are is other influence from other operations other than the quarry.

The meteorological data is not from weather stations near the quarry. The distance is between 40 and 120 kilometers from the site. These stations are at different locations to simulate the metrological data for the quarry Taivassalo. For this model it is the most representable for these two observation days. A recommendation for further research would be to also get the meteorological data at closer surroundings of the quarry. Preferably, this would be collected at the same time of the observation days and at the same level as the receptor points. The use of correct and improved meteorological data is required to improve the predictability of the dust dispersion in the future.

For improvement of the dust dispersion modeling could be looked into more receptor points in the quarry or open pit. In this study is only looked to the Gaussian plume model it could be valuable to consider the turbulence wind behavior. Furthermore, in this study is only looked at PM_{10} for the reason that the observed data was reliable. The AERMOD software could investigate also the TSP or $PM_{2.5}$. In this study, it would be interesting to see how the ratio acts between the different dust particles.

The dust dispersion figures from the Analyst software are interesting for the spread of the dust dispersion. The dust dispersion could be of value in the future to see in which areas the complication of dust will develop. The predicted areas of complication could be of help while planning, licensing and during operations on site. It could also give an indication of dangerous areas in the quarry with different weather circumstances.

References

AP-42, 2003. *Compilation of air pollutant emission factors Volume I: Stationary point and area sources,* North Carolina, United States: Office of Air Planning and Standards Office.

Appleton, T. J., Kingman, S. W., Lowndes, I. S. & Silvester, S. A., 2006. The development of a modelling strategy for the pit simulation of fugitive dust emissions from in-pit quarrying activities: a UK case study. *International Journal of Mining, Reclamation and Environment,* pp. 57-82.

Bangert, M. et al., 2012. Saharan dust event impacts on cloud formation and radiation over Western Europe. *Atmospheric Chemistry and Physics,* pp. 4045-4063.

Behera, S. N., Sharma, M., Dikshit, O. & Shukla, S. P., 2011. GIS-based Emission Inventory, Dispersion Modeling and Assessment for Source Contributions of Particulate Matter in an Urban Environment. *Water, Air and Soil Pollution 218,* pp. 423-436.

Bhandari, S., 2011. Modelling dust plume movement resulting from surface blasting operations. *EXPLO Conference Melbourne,* pp. 1-8.

Bruce, J., Smith, J., Datson, H. & Fowler, M., 2016. Modelling Dust Emissions from a Source Using Dust Monitoring and Meteorological Data. *Journal of Environmental Protection 7,* pp. 467-472.

Chakraborty, M. et al., 2002. Determination of the emission rate from various opencast mining operations. *Environmental Modelling and Software 17,* pp. 467-480.

Chang, C.-T., Chang, Y.-M., Lin, W.-Y. & Wu, M.-C., 2012. Fugitive dust emission source profiles and assessment of selected control strategies for particulate matter at gravel processing sites in Taiwan. *Journal of the Air and Waste Management Association,* pp. 1262-1268.

Chang, J. & Hanna, S., 2004. Air quality model performance evaluation. *Meteorology Atmospheric Physics,* Volume 87, pp. 167-196.

Chaulya, S., 2006. Emission rate formulae for surface iron mining activities. *Environmental Modeling Assessment,* Issue 11, pp. 361-370.

Chaulya, S. et al., 2002. Development of empirical formulae to determination of the emission rate from various opencast coal mining operations. *Environmental Modelling and Software 17,* pp. 467-480.

Chaulya, S., Chakraborty, M. & Singh, R., 2001. Air pollution modelling for a proposed limestone quarry. *Water, Air and Soil Pollution 126,* pp. 171-191.

Cimorelli, A. et al., 2004. AERMOD: A dispersion model for industrial source applications. Part I: General model formulation and boundary layer characterization. *Journal of applied meteorology,* Volume 44, pp. 682-693.

Colinet, J. F. et al., 2010. *Best Practice for Dust Control in Coal Mining,* Pittsburgh, PA: DHHS (NIOSH) Publication.

Collett, R. & Oduyemi, K., 1997. Air quality modelling: a technical review of mathematical approaches. *Meteorological Applications 4*, pp. 235-246.

Cooper, C. & Alley, F., 2010. *Air pollution control a design approach.* Fourth edition ed. Florida: Prospect Heights, IL : Waveland Press 2010.

Countess Environmental, 2006. *Western Regional Air Partnership's Fugitive Dust Handbook.* Westlake Village: WGA Contract No. 30204-111.

Cui, H. et al., 2011. A tracer experiment study to evaluate the CALPUFF real time application in near-field complex terrain setting. *Elsevier, Atmospheric Environment 45,* pp. 7525-7532.

Curci, G., 2015. Uncertainties of simulated aerosol optical properties induced by assumptions on aerosol physical and chemical properties: an AQMEII-2 perspective. *Atmospheric Environment, Volume 115,* pp. 541-552.

Dekking, F., Kraaikamp, C., Lopuhaä & Meester, L., 2005. *A modern introduction to probability and statistics, Understanding how and why.* Londen: Springer-Verlag.

Demirarslan, K. O., Çetin Doğruparmak, Ş. & Karademir, A., 2017. Evaluation of three pollutant dispersion models for environmental assessment of a district in Kocaeli, Turkey. *Global NEST Journal Vol 19,* pp. 1-12.

Directorate General for Environment, 2016. *Air Quality.* [Online] Available at: http://ec.europa.eu/environment/air/quality/legislation/time_extensions.html

EPA, 1995. *User's guide for the industrial source complex (ISC3) Dispersion Models,* Research Triangle Park, North Carolina 27711: U.S. Environmental Protection Agency.

EPA, 2004b. *User's guide for the AERMOD meteorological preprocessor (AERMET),* North Carolina, United States: EPA-454/B-03-002.

EPA, 2004c. *User's guide for the AERMOD terrain preprocessor (AERMAP),* North Carolina, United States: EPA-454/B-03-003.

EPA, 2013. *AERSURFACE User's Guide ,* Research Triangle Park, North Carolina: Office of Air Quality Planning and Standards, Air Quality Assessment Division, Air quality Modeling Group.

EPA, 2016. *AERMOD Model Formulation and Evaluation,* North Carolina: U.S. Environmental Protection Agency, Office of Air Quality Planning and Standards, Air Quality Assessment Division, Air Quality Modeling Group.

EPA, 2016. *User's Guide for the AMS/EPA Regulatory Model (AERMOD),* North Carolina, United States: EPA-454/B-16-011.

European Commission Report, 2000. *Guidance on Assessment under the EU Air Quality Directives - Final Draft,* s.l.: EC Report.

European Environment Agency, 2016. *Air quality in Europe,* Brussel: EEA.

European Parliament and the Council, 2008. Directive 2008/50/EC of the European Parliament and of the council of 21 May 2008 on ambient air quality and cleaner air for Europe. *Official Journal of the Europe Union 152,* pp. 1-44.

Fuzzi, S. et al., 2015. Particle matter, air quality and climate: lessons learned and future needs. *Atmospheric Chemistry and Physics,* pp. 8217-8299.

Ghannam, K. & El-Fadel, M., 2013. Emissions characterization and regulatory compliance at an industrial complex: An integrated MM5/CALPUFF approach. *Elsevier Atmospheric Environment 69,* pp. 159-169.

Gifford, F., 1961. The estimation of the dispersion of windborne material. *Meteorological Magazine ,* Volume 90, pp. 33-49.

Gifford, F., 1976. *Nuclear Safety 2,* pp. 68-86.

Hall, D. J. et al., 2000. *A Review of Dispersion Model Inter-comparison studies using ISC, R91, AERMOD and ADMS,* Bristol: Environment Agency.

Haustein, K. et al., 2015. Testing the performance of state-of-the-art dust emission schemes using DO4Models field data. *Geoscientific Model Development 8,* pp. 341-362.

Hinds, W. C., 1999. *Aerosol technology: properties, behavior, and measurement of airborne particles.* New York, US: John Wiley and Sons.

Holmes, N. S. & Morawska, L., 2006. A review of dispersion modelling and its application to the dispersion of particles: An overview of different dispersions models available. *Elsevier, Atmospheric Environment 40,* pp. 5902-5928.

Industrial Minerals Europe, 2010. *Occupational Exposure Limits – Respirable dust – FULL TABLE.* [Online] Available at: http://www.ima-europe.eu/content/occupational-exposure-limits-%E2%80%93-respirable-dust-%E2%80%93-full-table

Jones, T., Morgan, A. & Richards, R., 2003. Primary blasting in a limestone quarry: physicochemical characterization of dust clouds. In: *Mineralogy Magazine 67.* Middlesex, United Kingdom: Mineralogical Society, pp. 153-162.

Kaiser, J. et al., 2014. The MESSy aerosol submodel MADE3 (v2.0b): description and a box model test. *Geoscientific Model Development ,* Volume 7, pp. 1137-1157.

Lashgari, A. & Kecojevic, V., 2016. Comparative analysis of dust emission of digging and loading equipment in surface coal mining. *International Journal of Mining, Reclamation and Environment,* pp. 181-196.

Lazaridis, M., 2011. *First Principles of Meteorology and Air Pollution.* Chania, Greece: Springer Science and Business Media B.V..

Lownes, I., 2008. The application of an improved multi-scale computational modelling techniques to predict fugitive dust dispersion and deposition within and from surface operations. In: *Twelfth U.S./North American Mine Ventilation Symposium 2008.* Reno, Nevada: 12th U.S. North American Mine Ventilation Symposium 2008, pp. 359-366.

McElroy, J. & Pooler, F., 1968. *St. Louis dispersion volume II analysis.* Arlington, VA: USDHEW PHS, NAPCA.

Monin, A. & Obukhov, A., 2008. Basic layer of turbulent mixing in the surface layer of the atmosphere. *Trudy Geofizicheskogo Instituta, Alademiya Nauk SSSR,* pp. 163-187.

National Institute of Water and Atmospheric Research, 2004. *Good Practice Guide for Atmospheric Dispersion Modelling,* Wellington, New Zealand: Ministry for the Environment of Manatū Mō Te Taiao.

National Pollutant Inventory, 2014. *Emission estimation technique manual for mining and processing of Non-metallic minerals Version 2.1,* Canberra: Department of the Environment Australian Government.

National Pollution Inventory, 2012. *Emission estimation technique manual for mining,* Canberra: Commonwealth of Australia.

Neshuku, M. N., 2012. *Comparison of the performance of two atmospheric dispersion models (AERMOD and ADMS) for open pit mining sources of air pollution,* Pretoria, Gauteng, South Africa: University of Petoria.

Organisack, J. & Reed, R., 2004. Characteristics of fugitive dust generated from unpaved mine haulage roads. *International Journal of Mining, Reclamation and Environment 18,* pp. 236-252.

Orloff, K. G., Kaplan, B. & Kowalski, P., 2006. Hydrogen cyanide in ambient air near a gold heap leach field: Measured vs. modeled concentrations. *Atmospheric Environment,* pp. 3022-3029.

Petavratzi, E., Kingman, S. & Lowndes, I., 2005. Particulates from mining operations: A review of sources, effects and regulations. *Elsevier Minerals Engineering 18,* pp. 1183-1199.

Prabha, J. & Singh, G., 2006. Comparison and performance evaluation of dispersion models FDM and ISCST3 for a gold mine at Goa. *Jr. of Industrial Pollution Control 22,* pp. 297-303.

Reed, W., 2005. *Significant dust dispersion models for mining operations,* Cincinnati: National Institute for Occupational Safety and Health (NIOSH).

Sairanen, M. & Selonen, O., 2017. Dust formed during drilling in natural stone quarries. *Springer- Verlag Berlin Heidelberg 2017,* pp. 1-14.

Silvester, S., Lowndes, I. & Hargreaves, D., 2009. A computational study of particulate emissions from an open pit quarry under neutral atmospheric conditions. *Atmospheric Environment 43,* pp. 6415-6424.

Station, P. W., 2017. *Turku, Western Finland Monthly Climate Average, Finland.* [Online]
Available at: https://www.worldweatheronline.com/turku-weather-averages/western-finland/fi.aspx

Tartakovsky, D., Broday, D. & Stern, E., 2016. Evaluation of AERMOD and CALPUFF for predicting ambient concentrations of total suspended particle matter (TSP) emissions from a quarry in complex terrain. *Elsevier, Environmental Pollution 179,* pp. 138-145.

The United States Environmental Protection Agency, 2016. *Particle matter (PM) basics.* [Online]
Available at: https://www.epa.gov/pm-pollution/particulate-matter-pm-basics#PM

Trivedi, R., Chakraborty, M. & Tewary, B., 2009. Dust dispersion Modeling using fugitive dust model at an opencast coal project of Western Coalfields Limited, India. *Journal of Scientific & Industrial Research 68,* pp. 71-78.

Turner, B. D., 1970. *Workbook of atmospheric dispersion estimates.* Cincinnati, Ohio: Environmental Health Series.

Turnkey Instruments, L., 2017. *Environmental Monitor Training Manual.* [Online] Available at: http://www.turnkey-instruments.com/images/documents/Topas-Osiris-Monitor-Training-Manual.pdf

Vallero, A., 2008. *Fundamentals of air pollution.* Durham, North Carolina: Academic Press Elsevier.

Venkatram, A. et al., 2013. Re-formulation of plume spread for near-surface dispersion. *Atmospheric Environment ,* 77(Elsevier), pp. 846-855.

Visscher de, A., 2014. *Air modeling, foundations and applications.* New Jersey: John Wiley & Sons, Inc..

Vora, J., 2010. *Dust dispersion modeling for opencast mines,* India: National institute of technology Rourkela.

Wagenbrenner, S., Chung, S. & Lamb, B., 2017. A large source of dust missing in Particulate Matter inventories? Wind erosion of post-fire landscapes. *Elemanta, Science of the Anthropocene,* pp. 2-10.

World Health Organization, 1999. *Hazard prevention and control in the work environment: Airborne dust.* Geneva: s.n.

World Health Organization, 2006. *Air quality guidelines for particulate matter, ozone, nitrogen dioxide and sulfur dioxide,* Switzerland: WHO Press.

Zou, B., Zhan, F., Wilson, J. & Zeng, Y., 2010. Performance of AERMOD at different time scales. *Simulation modeling Practice and Theory 18,* Volume 18, pp. 612-623.

Appendix A

This appendix is constructed to get into detail for the Gaussian plume model. A Gaussian Plume model is a Gaussian model to determine the plume. The model assumes the plume independent of the wind and heights. The corrections of the wind speed can be changed at appropriate height into the model. (Visscher de, 2014)
Within the context of the Gaussian plume model, it is assumed that a plume released in the atmosphere is diluted by the following mechanisms:

Downwind: In the x direction the plume is diluted by the wind
Crosswind: In the y direction the plume is diluted by random motions of air parcels, such as eddies
Vertical wind: In the z-direction (vertical) the plume is diluted by random motions of air parcels. The spread of the plume is bounded by the ground and an elevated temperature inversion

While the dilution in the x direction is assumed to be the result of a non-random process (wind flow), the dilution in the y and z directions is the result of a random process, and the result will be a randomly fluctuating concentration. All we can hope to calculate with a Gaussian plume model is the Reynolds average concentration of the pollutant, R. The calculation of instantaneous concentrations is not the objective of a Gaussian plume model.

Considering the three dilution mechanisms outlined above, the Gaussian plume equation can be subdivided into three parts, each representing a dilution mechanism:

$$R = C_x \varphi_y \varphi_z \qquad \text{A. 1}$$

Where C_x = the pollution of plume (mg/m)
φ_y = lateral crosswind
φ_z = vertical wind

As a plume is emitted, it is diluted in the downwind direction by mixing with ambient air.

$$C_x = \frac{Q}{u_s} \qquad \text{A. 2}$$

Where C_x = pollution mass per meter of plume length (mg/m)
Q = mass emission rate (mg/s)
u_s = average wind speed (m/s)

When a plume moves downwind, it is diluted in the crosswind direction by turbulent eddies. If the dilution is the result of a large number of motions each having a negligible effect on the plume concentration profile, then the crosswind concentration profile follows a Gaussian probability density function:

$$\varphi_y = \frac{1}{\sqrt{2\pi}\sigma_y} \exp\left(-0.5 \frac{y^2}{\sigma_y^2}\right) \qquad \text{A. 3}$$

Where y = lateral crosswind distance from the plume axis (m), see Figure 7
σ_y = spread parameter in horizontal lateral direction (m)

The plume is also diluted in the vertical direction. The dilution mechanism is the same, but the extent of the dilution depends on the circumstances. If the dilution is unbounded, the vertical concentration profile also follows a Gaussian probability density function:

$$\varphi_z = \frac{1}{\sqrt{2\pi}\sigma_z} \exp\left[-0.5\frac{(z-h)^2}{\sigma_z^2}\right] \quad \text{A. 4}$$

Where z = height above the ground (m)
σ_z = spread parameter in the vertical direction (m)
h = effective source height (m)

Effective source height equation:

$$h = h_s + \Delta h \quad \text{A. 5}$$

Where h_s = stack height or source height
Δh = plume rise

The plume dispersion is always bounded by the ground surface. There is no plume to the ground, then the plume is reflected. The equation leads to the following probability density function:

$$\varphi_z = \frac{1}{\sqrt{2\pi}\sigma_z}\left\{\exp\left[-0.5\frac{(z-h)^2}{\sigma_z^2}\right] + \exp\left[-0.5\frac{(z+h)^2}{\sigma_z^2}\right]\right\} \quad \text{A. 6}$$

Combining equations A.1- A.3 and A.6, the classical Gaussian plume equation is obtained as shown in equation (2):

$$R = \frac{Q}{2\pi u_s \sigma_y \sigma_z} \exp\left(-0.5\frac{y^2}{\sigma_y^2}\right)\left\{\exp\left[-0.5\frac{(z-h)^2}{\sigma_z^2}\right] + \exp\left[-0.5\frac{(z+h)^2}{\sigma_z^2}\right]\right\} \quad \text{A. 7}$$

Appendix B

B.1: Overview Meteorological data

		Sensible Heat Flux	Friction Velocity	Mechanical Mixing Height	Monin-Obukov Length	Surface Roughness	Bowen Ratio	Albedo	Wind Speed[1]	Wind Direction	Temperature[2]	Relative Humidity	Station Pressure	Cloud Cover
DD/MM/YY	**Hr**	W/m^2	m/s	m	m	m	#	#	m/s	degree	K	%	mb	tenths
28/02/2013	**10:00-11:00**	4.6	0.384	574	-1094.0	0.228	0.50	0.57	3.6	289	278.1	65	1000	1
	11:00-12:00	16.8	0.443	706	-460.5	0.228	0.50	0.55	4.1	279	278.1	65	1000	5
	12:00-13:00	8.4	0.543	959	-1701.8	0.228	0.50	0.54	5.1	290	277.0	75	998	9
	MIN	4.6	0.384	574	-1701.8	0.228	0.50	0.54	3.6	279	277.0	65	998	1
	MAX	16.8	0.543	959	441.3	0.228	0.50	0.63	5.1	290	278.1	75	1001	9
	MEAN	3.2	0.452	734	-703.8	0.228	0.50	0.57	4.2	284	277.6	69	1000	4
01/03/2013	**07:00-08:00**	-62.1	0.615	1157	415.6	0.429	0.52	1.00	4.6	12	274.2	86	991	10
	08:00-09:00	-36.0	0.429	708	202.8	0.332	0.52	0.48	3.6	358	274.2	86	992	10
	09:00-10:00	-10.9	0.440	700	693.2	0.332	0.52	0.33	3.6	354	274.2	86	993	10
	10:00-11:00	3.3	0.586	1075	-5465.4	0.429	0.52	0.25	4.6	14	274.2	86	994	10
	MIN	-62.1	0.429	700	-5465.4	0.332	0.52	0.25	3.6	12	274.2	86	989	10
	MAX	3.3	0.615	1157	693.2	0.429	0.52	1.00	4.6	358	274.2	86	994	10
	MEAN	-33.54	0.537	960	-747.64	0.390	0.52	0.612	4.2	151	274.2	86	992	10

[1] Reference height for the wind speed is 2 meter
[2] Reference height for the Temperature is 10 meter

Overview hourly wind rose of 28/02/2013

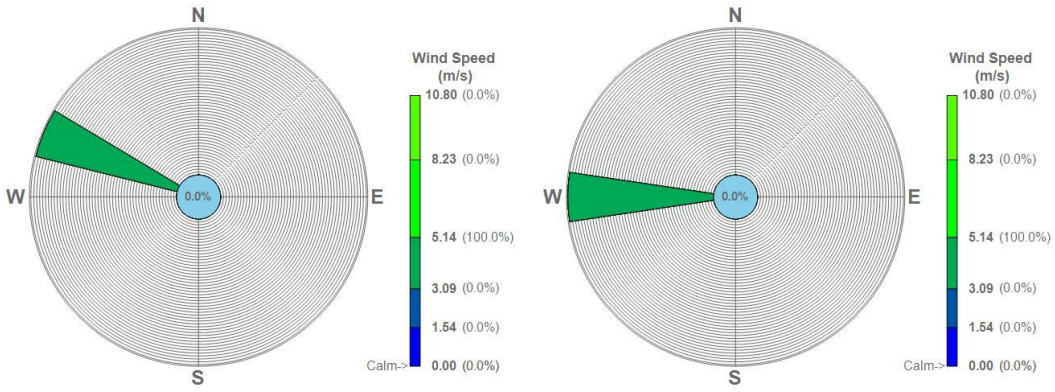

B_1: Wind rose of 28/02/2013 10:00-11:00 (left) wind rose of 28/02/2013 11:00-12:00 (right)

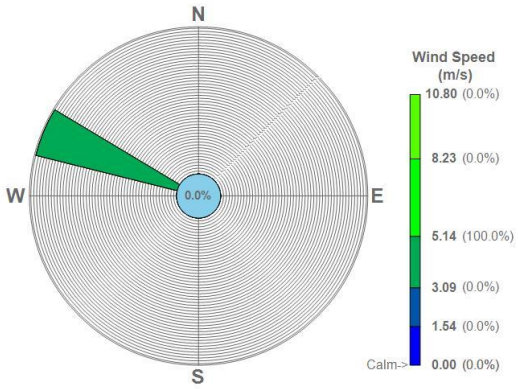

B_2: Wind rose of 28/02/2013 12:00-13:00

Overview hourly wind rose of 01/03/3013

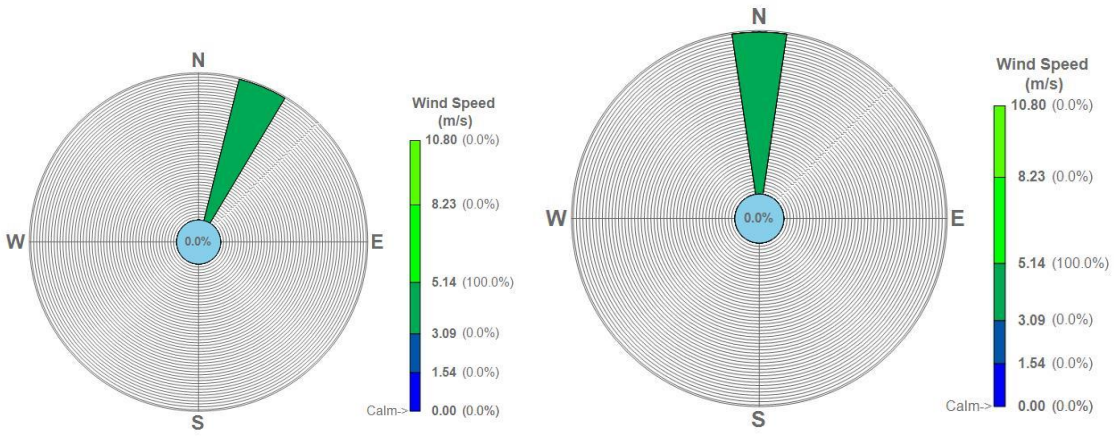

B_3: Wind rose 01/03/2013 07:00-08:00 (left) wind rose 01/03/2013 08:00-09:00 (right)

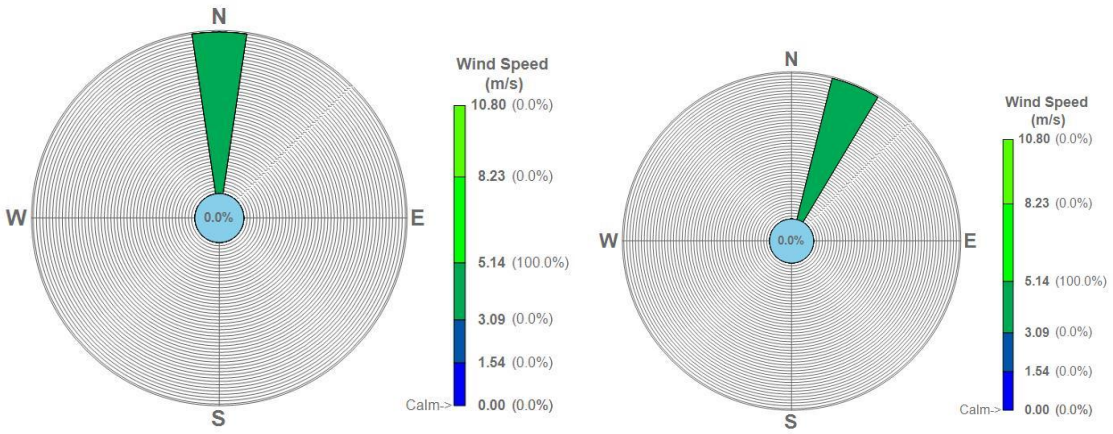

B_4: Wind rose 01/03/2013 09:00-10:00 (left) wind rose 01/03/2013 10:00-11:00 (right)

Appendix C

C.1: 28/02/2013 Raw predicted data of the receptors

	10.00-11.00				
	R5	**R10**	**R20**	**R30**	**R40**
Observed	215.65	39.02	23.47	17.77	17.60
Case 1	12577.89	4263.92	972.96	440.04	244.66
Case 2	12649.71	4329.67	1257.36	758.11	573.90
Case 3	10134.13	3476.89	1062.77	670.10	524.97
Case 4	12057.78	4024.71	1187.97	725.44	552.92

11.00-12.00		
R5	**R10**	**R50**
742.18	257.39	38.12
8915.20	2970.07	97.90
8981.28	3031.35	434.07
7221.28	2445.01	414.75
8914.63	2932.27	425.86

12.00-13.00	
R5	**SW10**
306.17	414.44
9668.19	0.00
9732.67	68.30
7865.22	68.30
9230.59	67.08

C.2: 01/03/2013 Raw predicted data of the receptors

	07.00-08.00		
	R5	**R10**	**SW10**
Observed	77.42	35.62	120.80
Case 1	12890.02	4369.73	0.00
Case 2	162.25	228.66	2388.33
Case 3	162.25	228.66	2388.33
Case 4	127.30	217.02	2845.7

08.00-09.00				
R5	**R10**	**R20**	**R30**	**R40**
326.21	75.86	89.97	22.54	24.67
12890.02	4369.73	997.11	450.96	250.73
585.38	446.65	325.72	233.87	208.19
585.38	446.65	325.72	233.87	208.19
389.59	346.30	307.32	227.48	205.71

09.00-10.00	
R5	**R40**
326.21	27.44
12577.89	244.66
1375.23	209.77
1375.23	209.77
991.54	204.58

10.00-11.00		
R5	**R50**	**R60**
300.65	31.76	34.80
12577.89	153.97	106.36
140.78	187.47	259.63
140.78	187.47	259.63
116.87	195.16	281.65

Appendix D

D.1: Hourly overview for sensitivity analyses of Monin-Obukov Length and Surface Roughness

		Monin-Obukov Length			Surface Roughness		
		(m)	Range		(m)	Range	
DD/MM/YY	hr:min	Normal state	Min	Max	Normal state	Min	Max
28/02/2013	10:00-11:00	-1094	-246	-2188	0.228	0.057	0.456
	11:00-12:00	-461	-115	-921	0.228	0.057	0.456
	12:00-13:00	-1702	-425	-3404	0.228	0.057	0.456
03/01/2013	07:00-08:00	416	104	831	0.429	0.107	0.858
	08:00-09:00	203	51	406	0.332	0.083	0.664
	09:00-10:00	693	173	1386	0.332	0.083	0.664
	10:00-11:00	-5465	-1366	-10931	0.429	0.107	0.858

D.2: Hourly overview for sensitivity analyses of Bowen Ratio and Albedo

		Bowen Ratio			Albedo		
		#	Range		#	Range	
DD/MM/YY	hr:min	Normal state	Min	Max	Normal state	Min	Max
28/02/2013	10:00-11:00	0.50	0.13	1.00	0.57	0.14	1.14
	11:00-12:00	0.50	0.13	1.00	0.55	0.14	1.10
	12:00-13:00	0.50	0.13	1.00	0.54	0.14	1.08
03/01/2013	07:00-08:00	0.52	0.13	1.04	1.00	0.25	2.00
	08:00-09:00	0.52	0.13	1.04	0.48	0.12	0.96
	09:00-10:00	0.52	0.13	1.04	0.33	0.08	0.66
	10:00-11:00	0.52	0.13	1.04	0.25	0.06	0.50

D.3: Hourly overview for sensitivity analyses for the Emission Factor and Wind Speed

		Emission Factor			**Wind Speed**		
		(g/s)	**Range**		**(m/s)**	**Range**	
DD/MM/YY	**hr:min**	**Normal state**	**Min**	**Max**	**Normal state**	**Min**	**Max**
28/02/2013	**10:00-11:00**	0.264	0.013	0.527	3.6	1	8
	11:00-12:00	0.267	0.013	0.534	4.1	1	9
	12:00-13:00	0.273	0.014	0.546	5.1	1	11
03/01/2013	**07:00-08:00**	0.270	0.068	0.540	4.6	1	10
	08:00-09:00	0.264	0.066	0.527	3.6	1	8
	09:00-10:00	0.264	0.066	0.527	3.6	1	8
	10:00-11:00	0.270	0.068	0.540	4.6	1	10

Appendix E

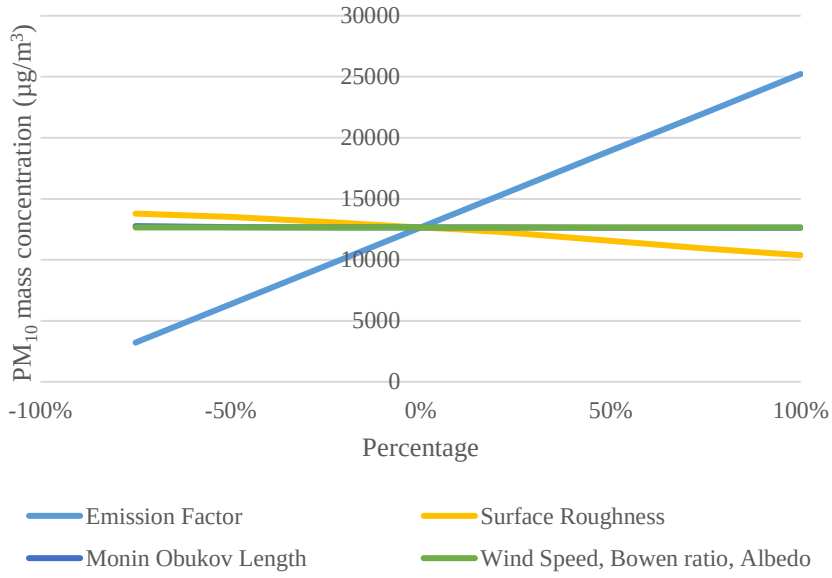

E_1: 28/02/2013 10:00-11:00 Receptor point 5m

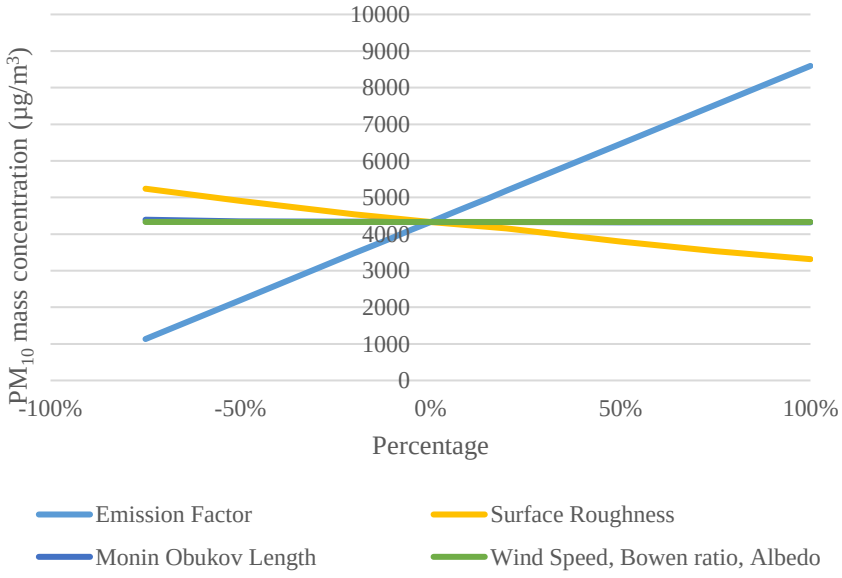

E_2: 28/02/2013 10:00-11:00 Receptor point 10m

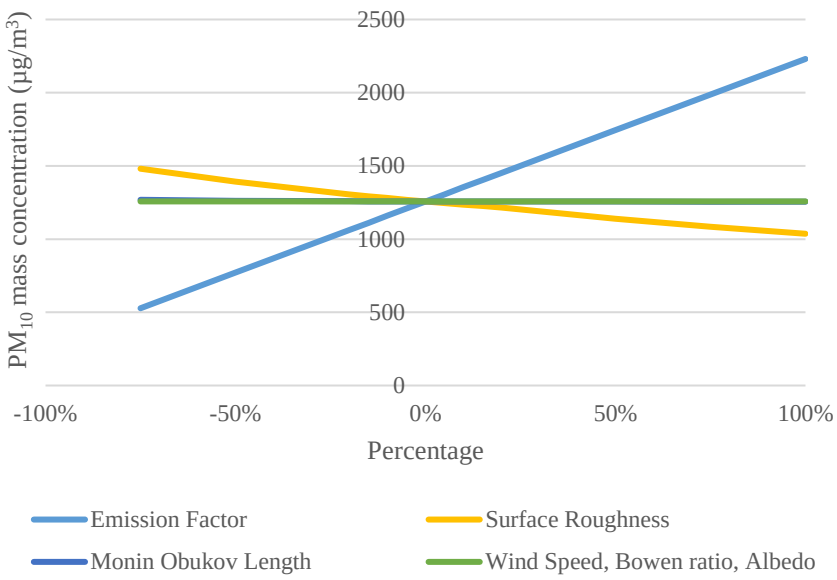

E_3: 28/02/2013 10:00-11:00 Receptor point 20m

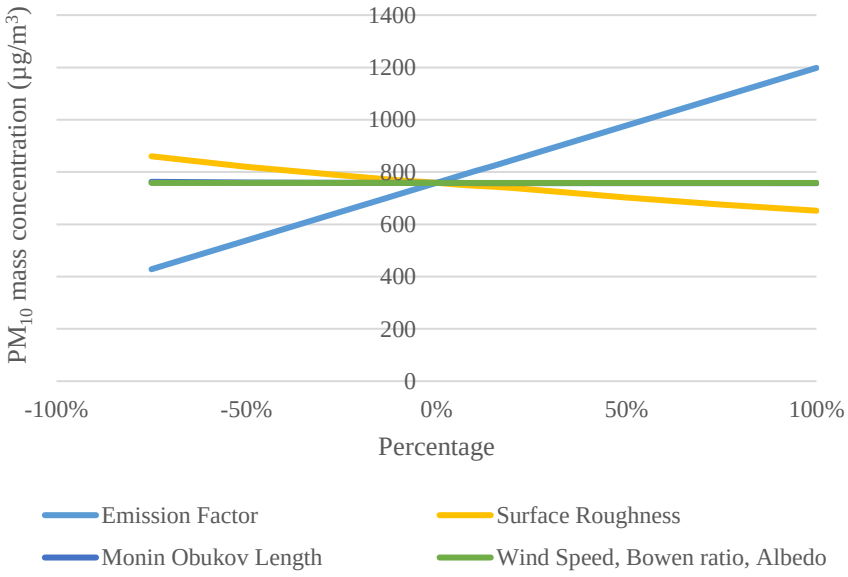

E_4: 28/02/2013 10:00-11:00 Receptor point 30m

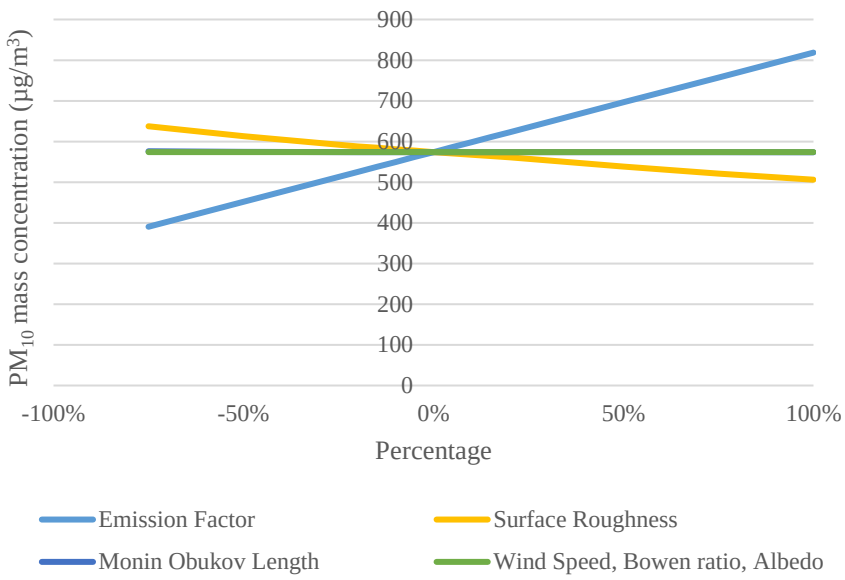

E_5: 28/02/2013 10:00-11:00 Receptor point 40m

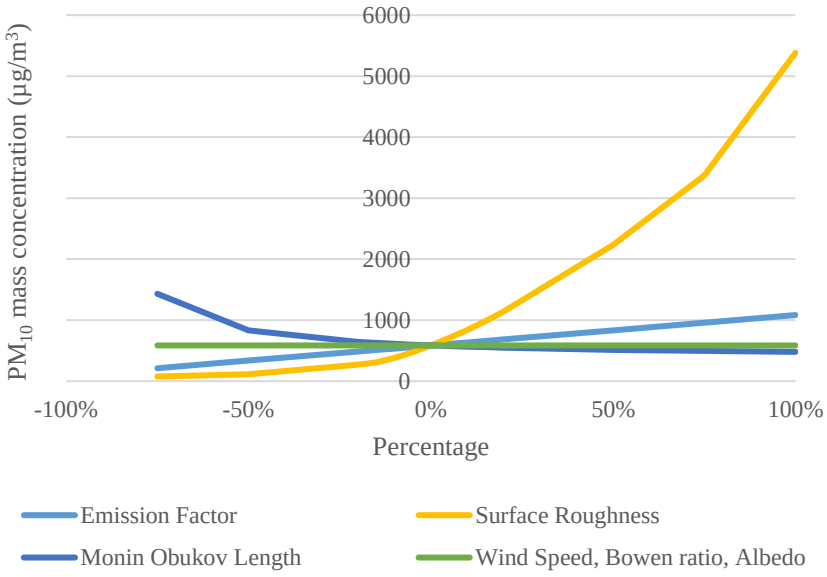

E_6: 01/03/2013 08:00-09:00 Receptor point 5m

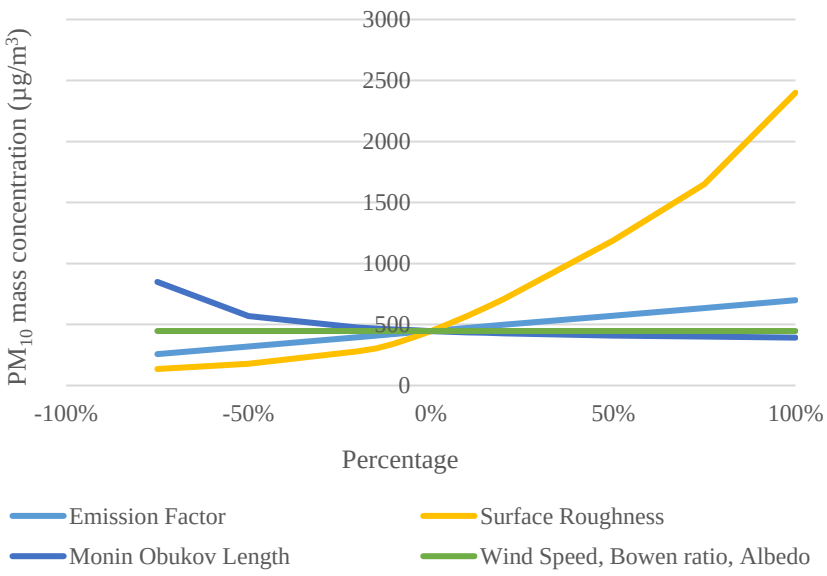

E_7: 01/03/2013 08:00-09:00 Receptor point 10m

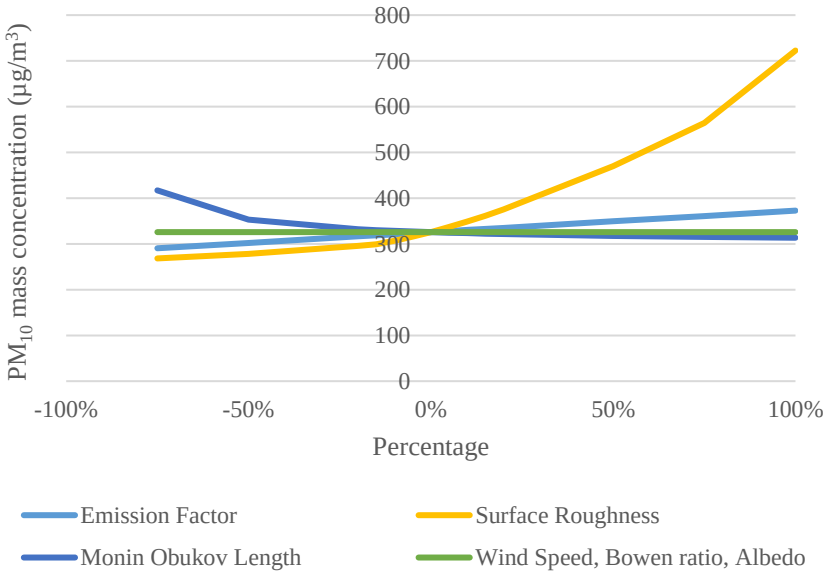

E_8: 01/03/2013 08:00-09:00 Receptor point 20m

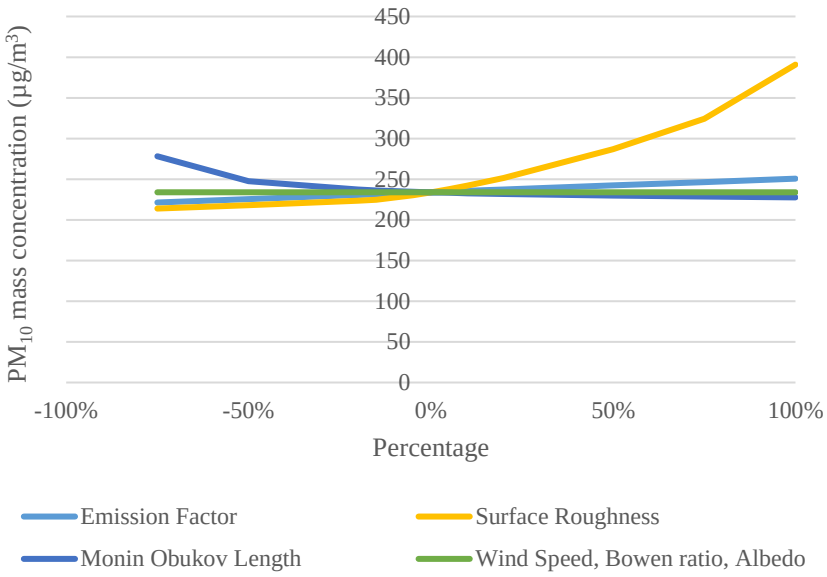

E_9: 01/03/2013 08:00-09:00 Receptor point 30m

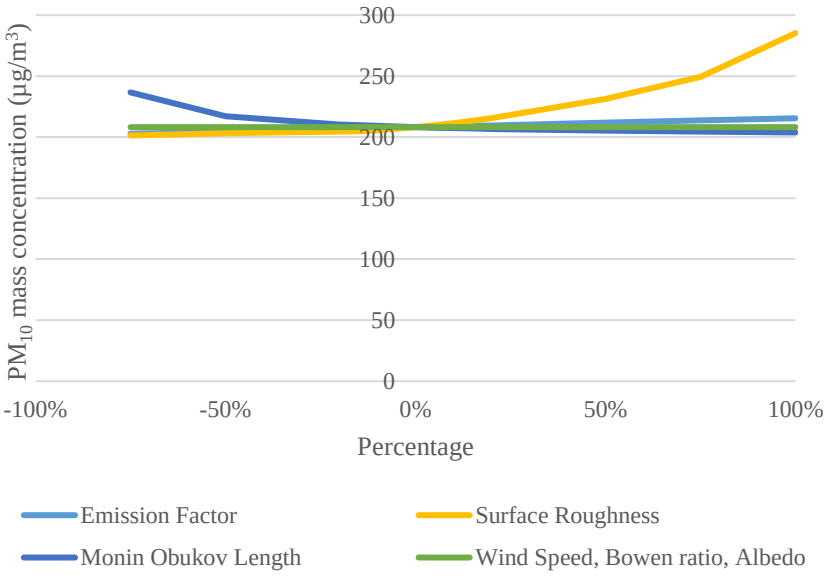

E_10: 01/03/2013 08:00-09:00 Receptor point 40m

Sensitivity analyses Surface Roughness and Monin-Obukov length

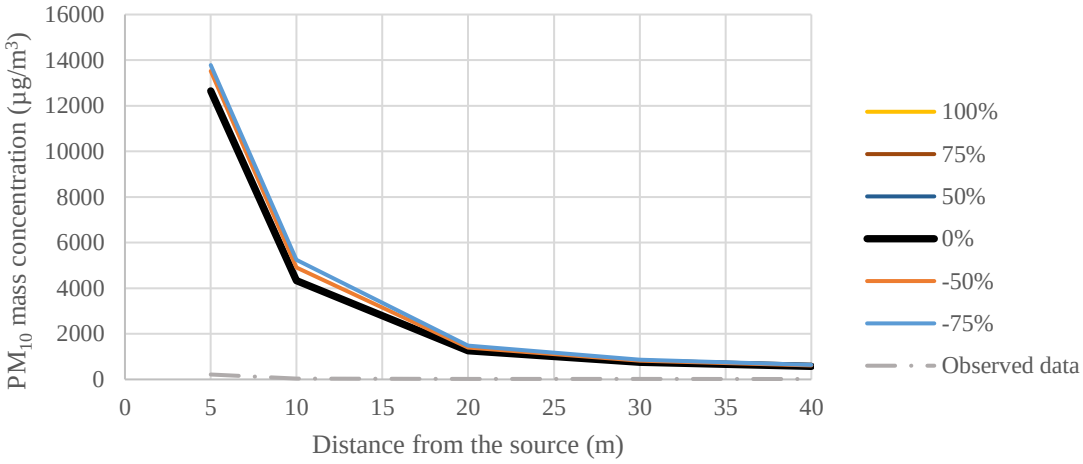

E_11: Sensitivity analyses 28/02/2013 case 2 for Surface Roughness and the observed data

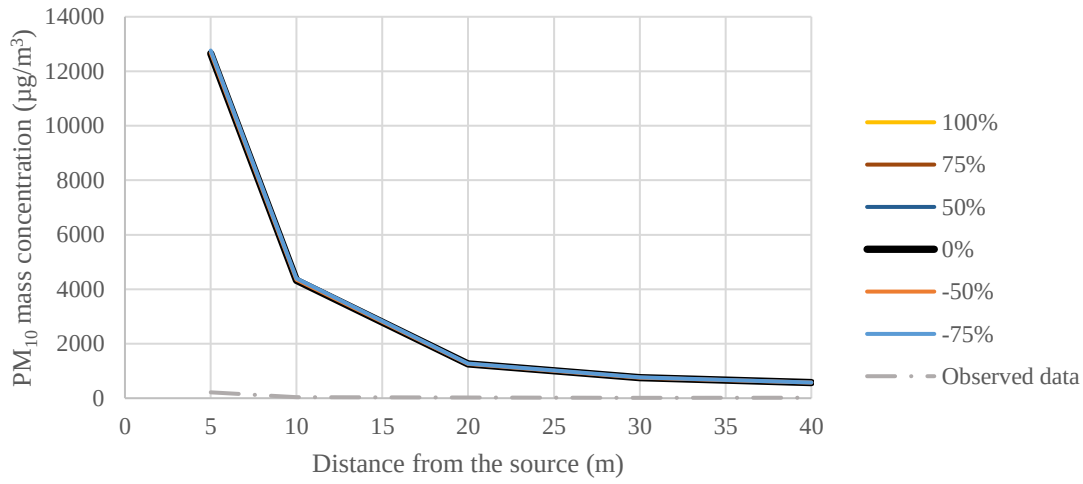

E_12: Sensitivity analyses 28/02/2013 case 2 for Monin-Obukov length and the observed data

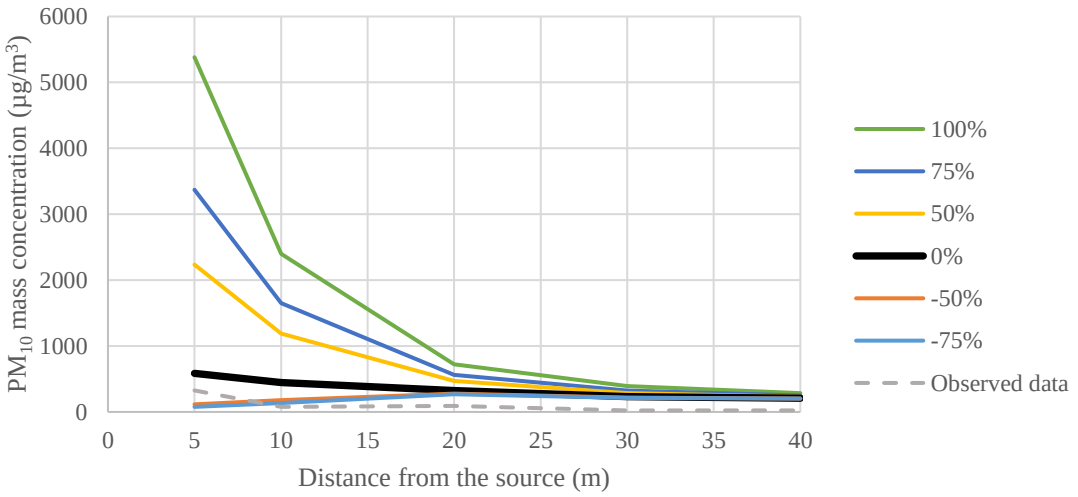

E_13: Sensitivity analyses 01/03/2013 case 2 for Surface Roughness and the observed data

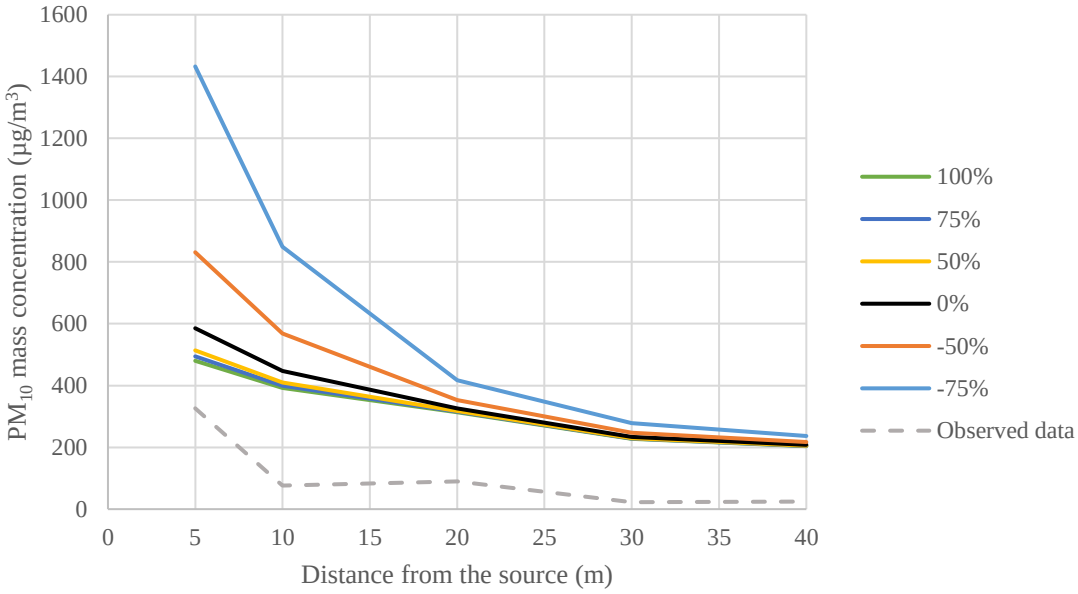

E_14: Sensitivity analyses 01/03/2013 case 2 for Monin-Obukov length and the observed data

Appendix F

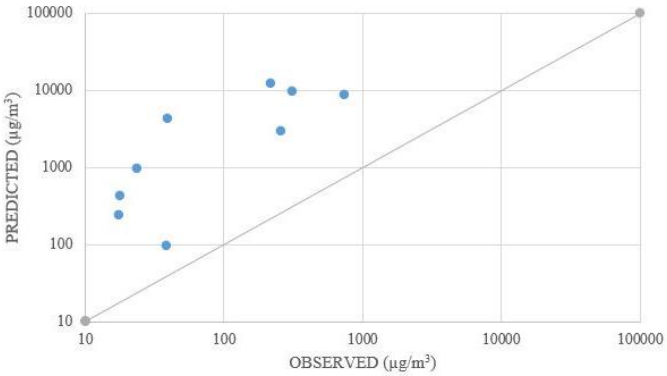

F_1: Q-Q plot 28/02/2013 for Observed and case 1

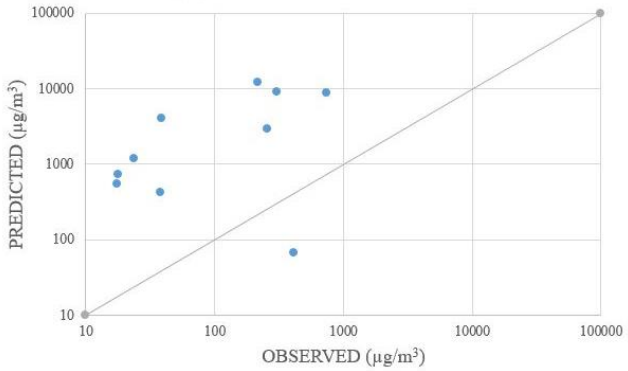

F_2: Q-Q plot 28/02/2013 for Observed and case 4

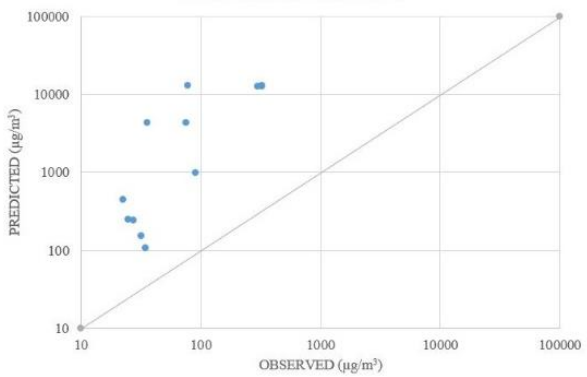

F_3: Q-Q plot 01/03/2013 for Observed and case

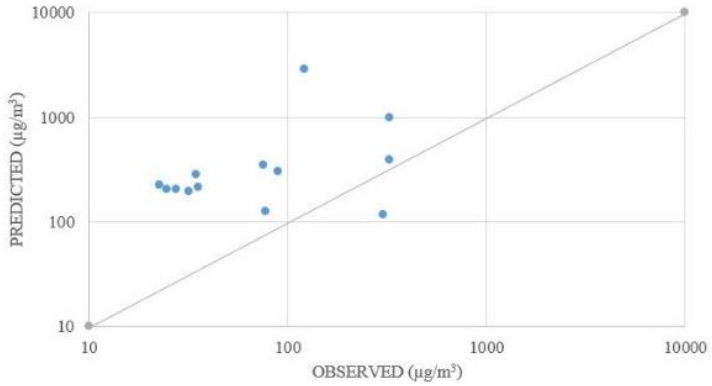

F_4: Q-Q plot 01/03/2013 for Observed and case 4

Appendix G

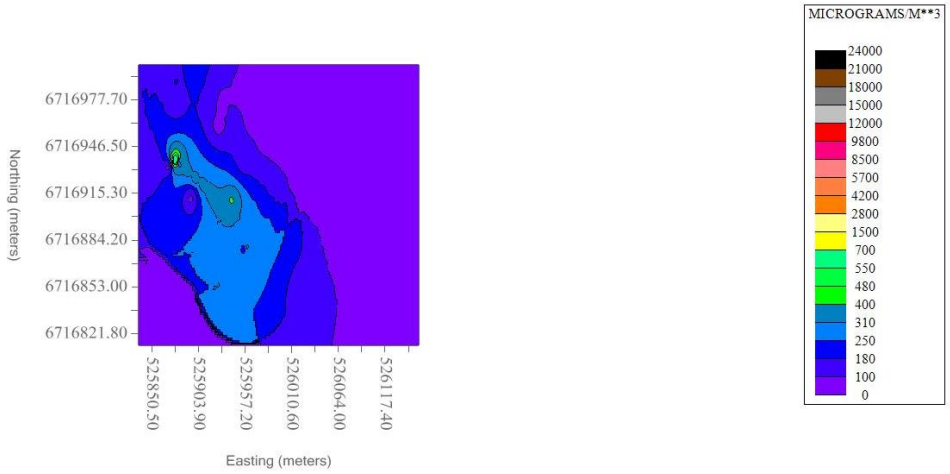

G_1: 28/02/2013 10:00-11:00 -95% Emission Factor

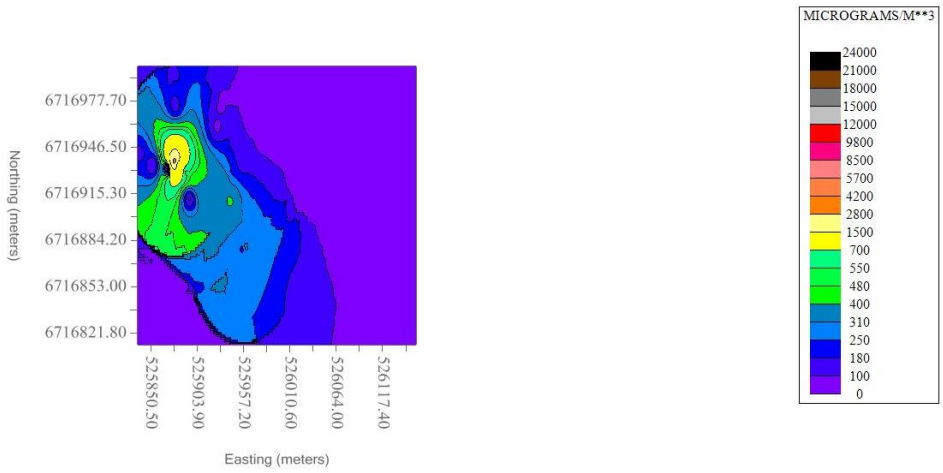

G_2: 28/02/2013 10:00-11:00 -75% Emission Factor

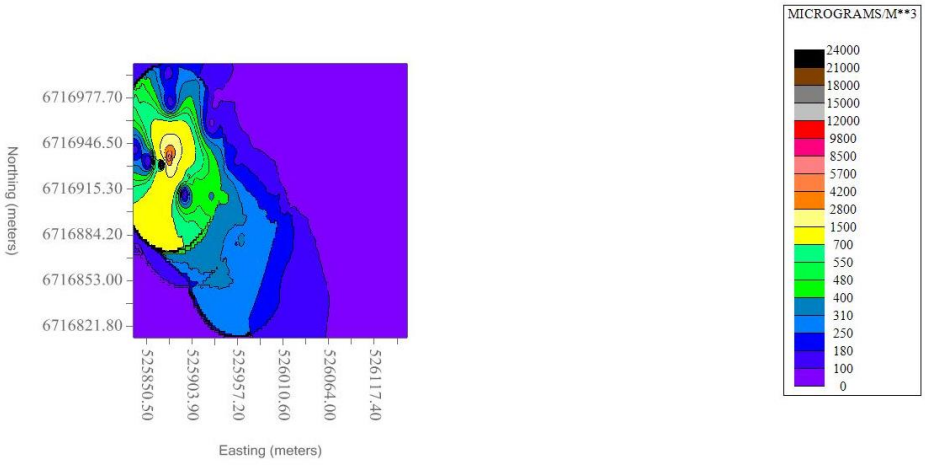

G_3: 28/02/2013 10:00-11:00 -50% Emission Factor

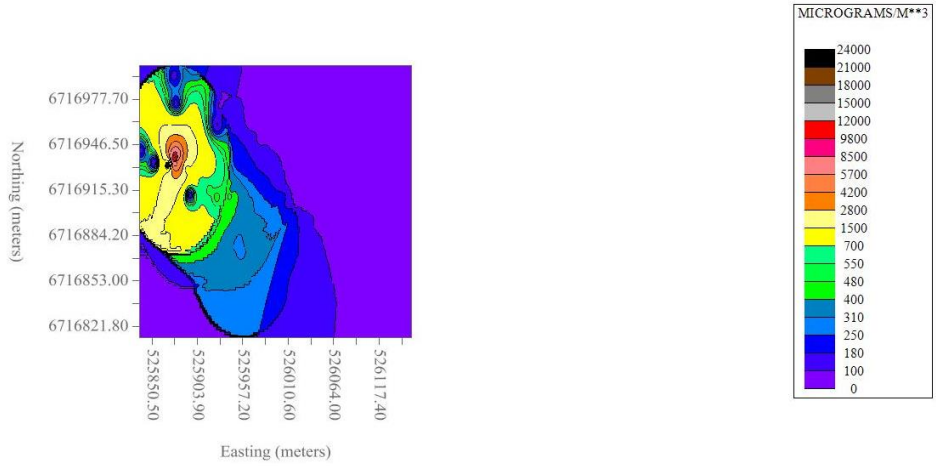

G_4: 28/02/2013 10:00-11:00 0% Emission Factor

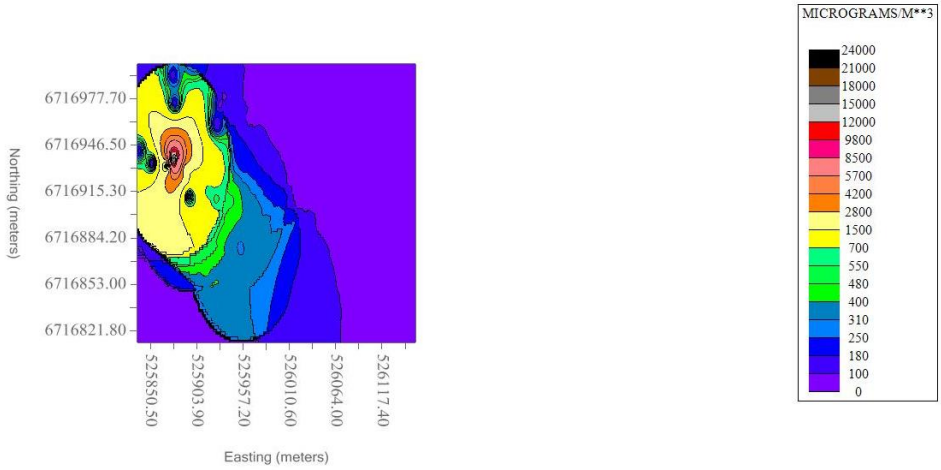

G_5: 28/02/2013 10:00-11:00 50% Emission Factor

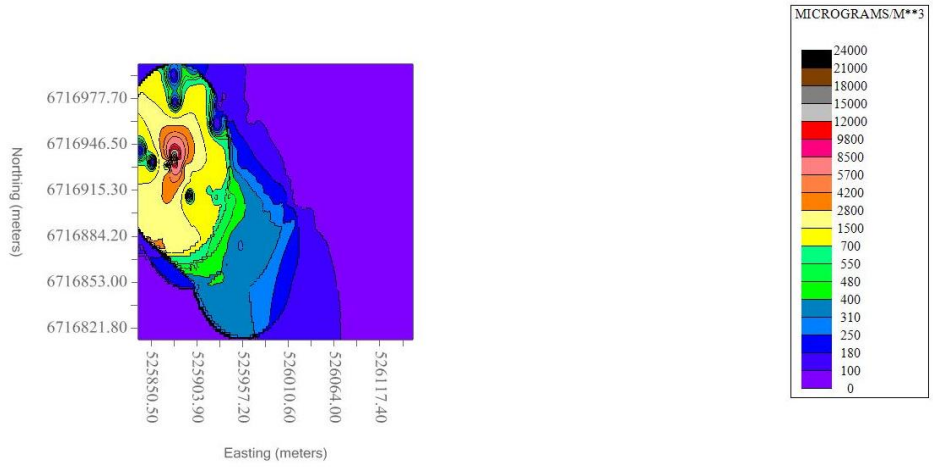

G_6: 28/02/2013 10:00-11:00 75% Emission Factor

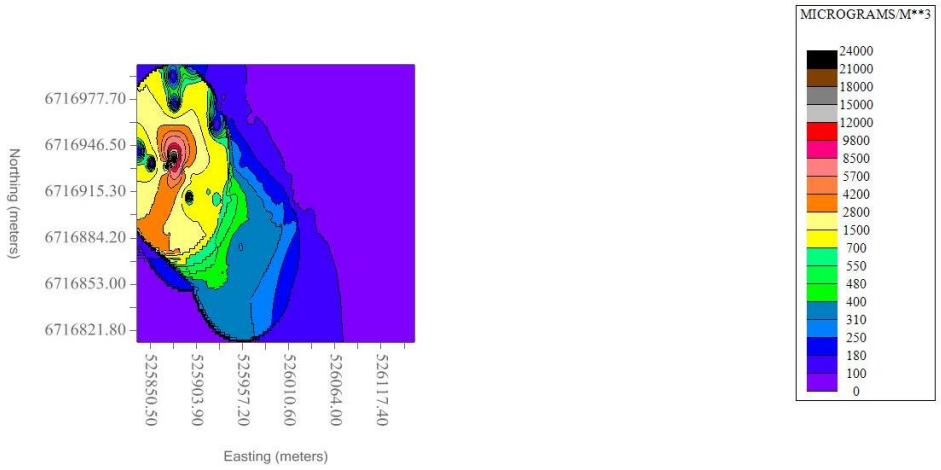

G_7: 28/02/2013 10:00-11:00 100% Emission Factor

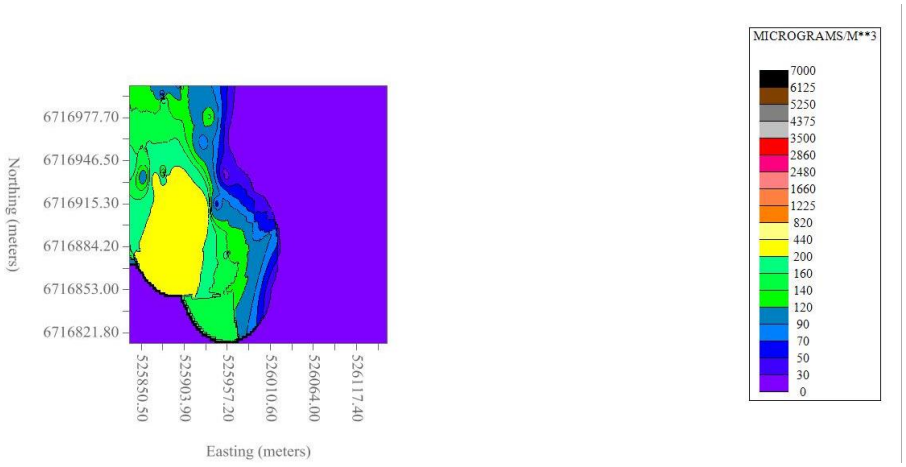

G_8: 01/03/2013 08:00-09:00 -95% Emission factor

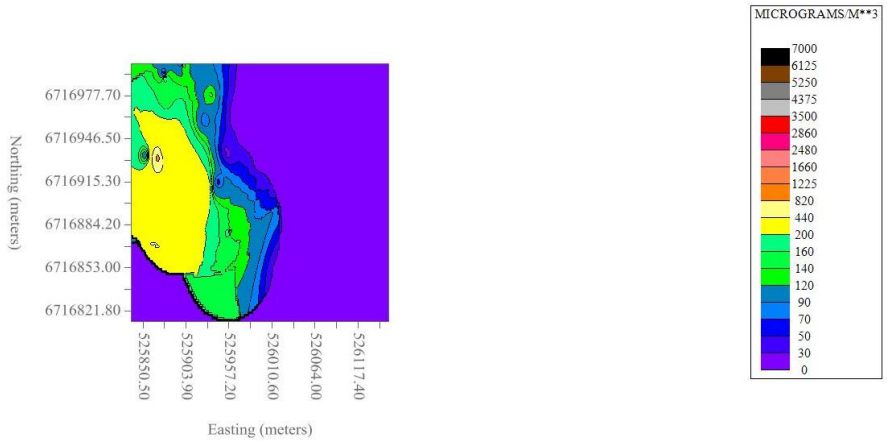

G_9: 01/03/2013 08:00-09:00 -75% Emission factor

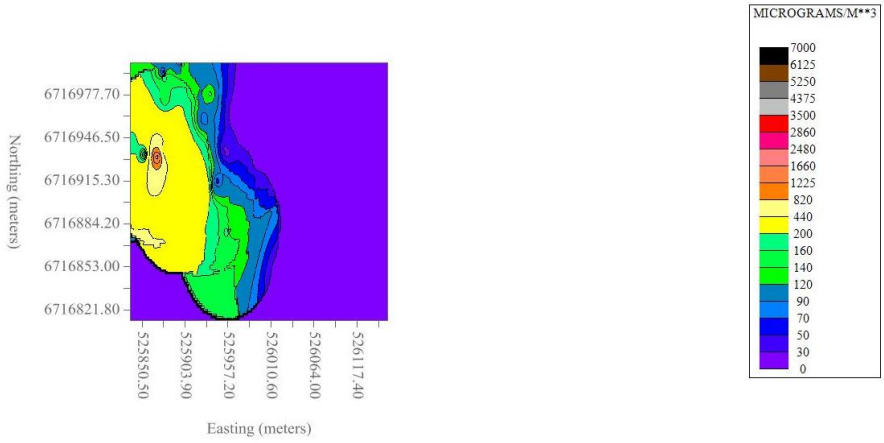

G_10: 01/03/2013 08:00-09:00 -50% Emission factor

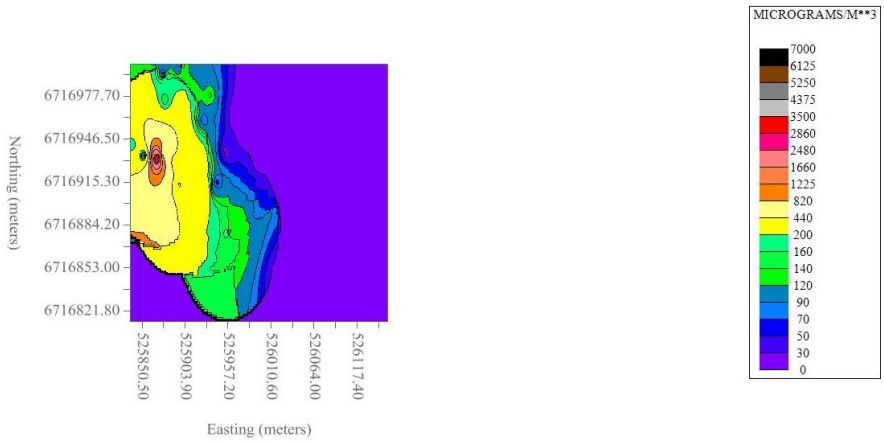

G_11: 01/03/2013 08:00-09:00 0% Emission factor

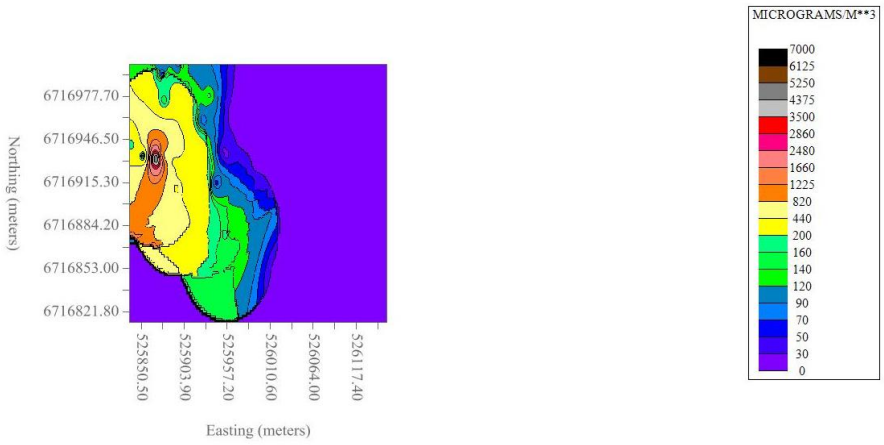

G_12: 01/03/2013 08:00-09:00 50% Emission factor

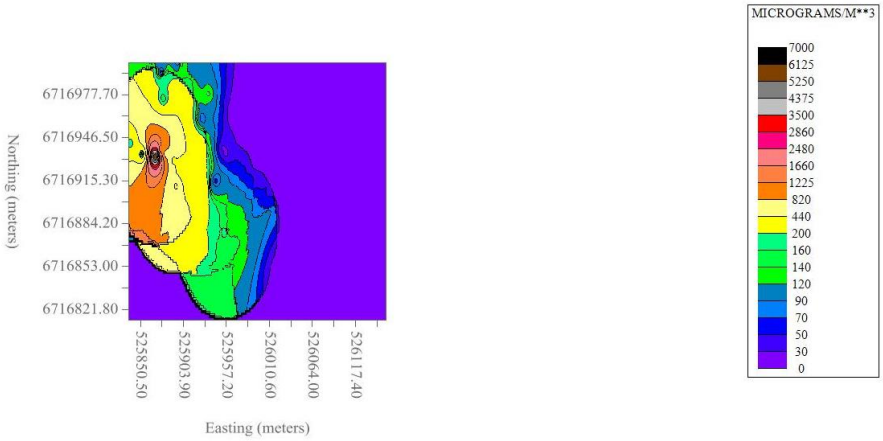

G_13: 01/03/2013 08:00-09:00 75% Emission factor

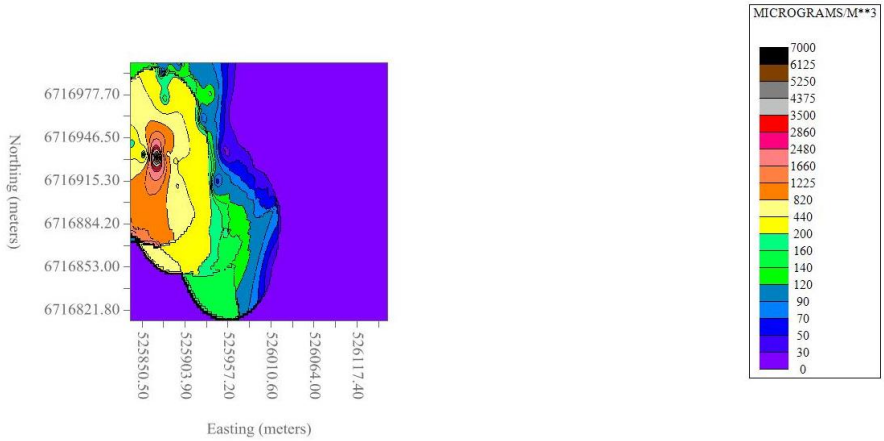

G_14: 01/03/2013 08:00-09:00 100% Emission factor